AD NUMBER

AD820329

LIMITATION CHANGES

TO:

Approved for public release; distribution is unlimited.

FROM:

Distribution authorized to U.S. Gov't. agencies and their contractors; Critical Technology; JUN 1967. Other requests shall be referred to Air Force Cambridge Research Laboratory, Hanscom AFB, MA 01730. This document contains export-controlled technical data.

AUTHORITY

AFCRL ltr dtd 22 Dec 1971

AFCRL-67-0473

STUDY TO OBTAIN DESIGN DATA FOR REENTRY ECM ANTENNA SYSTEMS(U)

VOLUME I OF 2

P.E. Bisbing, A.K. Jordan, D.L. McMenamin
W. Sawchuk, P. Scherer

REENTRY SYSTEMS DEPARTMENT
MISSILE AND SPACE DIVISION
GENERAL ELECTRIC COMPANY
P. O. BOX 8555, PHILA., PA. 19101

Contract No. F 19628-67-C-0210
Project No. 8671

First Quarterly Technical Report

CONTRACT MONITOR: WALTER ROTMAN
MICROWAVE PHYSICS LABORATORY

GE Report No. 67SD5232 June 1967

Sponsored By

ADVANCED RESEARCH PROJECTS AGENCY
DEPARTMENT OF DEFENSE
PROJECT DEFENDER
ARPA ORDER NO. 693, AMENDMENT NO. 1

Prepared For

AIR FORCE CAMBRIDGE RESEARCH LABORATORIES
OFFICE OF AEROSPACE RESEARCH
UNITED STATES AIR FORCE
BEDFORD, MASSACHUSETTS 01730

AFCRL-67-0473

STUDY TO OBTAIN DESIGN DATA FOR REENTRY ECM ANTENNA SYSTEMS(U)

VOLUME I OF 2

P.E. Bisbing, A.K. Jordan, D.L. McMenamin
W. Sawchuk, P. Scherer

REENTRY SYSTEMS DEPARTMENT
MISSILE AND SPACE DIVISION
GENERAL ELECTRIC COMPANY
P. O. BOX 8555, PHILA., PA. 19101

Contract No. F 19628-67-C-0210
Project No. 8671

First Quarterly Technical Report

CONTRACT MONITOR: WALTER ROTMAN
MICROWAVE PHYSICS LABORATORY

GE Report No. 67SD5232 June 1967

Sponsored By

ADVANCED RESEARCH PROJECTS AGENCY
DEPARTMENT OF DEFENSE
PROJECT DEFENDER
ARPA ORDER NO. 693, AMENDMENT NO. 1

Prepared For

AIR FORCE CAMBRIDGE RESEARCH LABORATORIES
OFFICE OF AEROSPACE RESEARCH
UNITED STATES AIR FORCE
BEDFORD, MASSACHUSETTS 01730

ACKNOWLEDGEMENT

This research was supported by the Advanced Research Projects Agency, Project DEFENDER, and was monitored by the Air Force Cambridge Research Laboratories, under Contract No. F19628-67-C-0210.

ABSTRACT

This report is the first quarterly technical report under this study of reentry effects associated with the transmission of electronic countermeasure (ECM) signals. Illustrative results for the aerothermochemical properties are presented for typical slender-body reentry conditions. These results were obtained from an approximate nonequilibrium inviscid shock layer flow field solution, which utilizes a combination of reacting streamtube and equilibrium flow field solutions. A discussion of the calculation method is included.

Literature surveys in the area of theory of antennas and propagation are summarized. (Types of ECM antennas in common use are discussed in Volume II.) Methods of calculating near-field distributions of antennas are discussed in a general way. Theoretical analyses of linear plasma effects are surveyed. Antenna breakdown is considered in terms of both the static air environment and the reentry environment. The theories of nonlinear propagation effects are summarized and finally a review of some alleviation techniques is given.

In general, it appears that nearly all of the important reentry effects on antennas and propagation can be reasonably well characterized using existing theory. However, parametric evaluation using these theories will have to be completed before this conclusion can be affirmed.

TABLE OF CONTENTS

Section		Page
1	INTRODUCTION	1-1
2	FLOW FIELD ANALYSIS	2-1
	2.1 Equilibrium Inviscid Flow Field Solution	2-1
	2.2 Nonequilibrium Streamtube Solution	2-2
	2.3 Results	2-4
	2.4 Future Flow Field Work	2-41
3	ANTENNAS AND PROPAGATION	3-1
	3.1 Antennas	3-1
	3.1.1 ECM Antennas	3-1
	3.1.2 Antenna Field Theory	3-1
	3.2 Linear Plasma Effects	3-4
	3.3 Antenna Breakdown	3-10
	3.3.1 Static Breakdown	3-10
	3.3.2 Reentry Effects	3-16
	3.4 Nonlinear Attenuation and Distortion	3-19
	3.4.1 Infinite Plasma Medium	3-21
	3.4.2 Semi-Infinite Plasma	3-26
	3.4.3 Plasma Slab	3-28
	3.5 Alleviation Techniques	3-29
4	CONCLUSION	4-1
5	REFERENCES	5-1

LIST OF ILLUSTRATIONS

Figure		Page
2.3-1	Streamwise Variation of Normalized Pressure vs Normalized Coordinate Along Body Surface	2-10
2.3-2	Streamwise Variation of Normalized Temperature vs Normalized Coordinate along Body Surface	2-11
2.3-3	Streamwise Variation of Normalized Density vs Normalized Coordinate Along Body Surface	2-12
2.3-4	Streamwise Variation of Normalized Velocity Parallel to Surface vs Normalized Coordinate Along Body Surface	2-13
2.3-5	Streamwise Variation of Molecular Oxygen Number Density vs Normalized Coordinate Along Body Surface	2-14
2.3-6	Streamwise Variation of Molecular Nitrogen Number Density vs Normalized Coordinate Along Body Surface	2-15
2.3-7	Streamwise Variation of Atomic Nitrogen Number Density vs Normalized Coordinate Along Body Surface	2-16
2.3-8	Streamwise Variation of Atomic Oxygen Number Density vs Normalized Coordinate Along Body Surface	2-17
2.3-9	Streamwise Variation of Nitric Oxide Number Density vs Normalized Coordinate Along Body Surface	2-18
2.3-10	Streamwise Variation of Electron Number Density vs Normalized Coordinate Along Body Surface	2-19
2.3-11	Normalized Pressure vs Shock Layer Thickness; $s_b/R_N = 4.962^{\backslash 1}$; Nonequilibrium	2-20
2.3-12	Normalized Pressure vs Shock Layer Thickness; $s_b/R_N = 6.125^{\backslash +1}$; Nonequilibrium	2-21
2.3-13	Normalized Pressure vs Shock Layer Thickness; $s_b/R_N = 2.433^{\backslash +2}$; Nonequilibrium	2-22
2.3-14	Normalized Temperature vs Shock Layer Thickness; $s_b/R_N = 4.962^{\backslash -1}$; Nonequilibrium	2-23
2.3-15	Normalized Temperature vs Shock Layer Thickness; $s_b/R_N = 6.125^{\backslash +1}$; Nonequilibrium	2-24
2.3-16	Normalized Temperature vs Shock Layer Thickness; $s_b/R_N = 2.433^{\backslash +2}$; Nonequilibrium	2-25
2.3-17	Normalized Density vs Shock Layer Thickness; $s_b/R_N = 4.962^{\backslash -1}$	2-26
2.3-18	Normalized Density vs Shock Layer Thickness; $s_b/R_N = 6.125^{\backslash 1}$	2-27
2.3-19	Normalized Density vs Shock Layer Thickness; $s_b/R_N = 2.433^{\backslash 2}$	2-28
2.3-20	Normalized Velocity Parallel to Surface vs Shock Layer Thickness; $s_b/R_N = 4.962^{\backslash -1}$	2-29
2.3-21	Normalized Velocity Parallel to Surface vs Shock Layer Thickness; $s_b/R_N = 6.125^{\backslash 1}$	2-30

LIST OF ILLUSTRATIONS (Cont)

Figure		Page
2.3-22	Normalized Velocity Parallel to Surface vs Shock Layer Thickness; $s_b/R_N = 2.433^{\backslash 2}$	2-31
2.3-23	Electron Number Density vs Shock Layer Thickness; $s_b/R_N = 4.962^{\backslash -1}$	2-32
2.3-24	Electron Number Density vs Shock Layer Thickness; $s_b/R_N = 6.125^{\backslash 1}$	2-33
2.3-25	Electron Number Density vs Shock Layer Thickness; $s_b/R_N = 2.433^{\backslash 2}$	2-34
2.3-26	$\int_0^{Y_{SN}} N_e \, dy$ vs Normalized Coordinate Along Body Surface; Nonequilibrium	2-35
3.2-1	Steepest Descent Contour C	3-7

LIST OF TABLES

Table		Page
2.3-1	Free Stream Conditions	2-5
2.3-2	Reaction System	2-6
2.3-3	Summary of Geometric Variables for Selected Body Surface Normals	2-8
2.3-4	Altitude Dependence of the Species Number Density Normal Profiles, $s_b/R_N = 4.962^{\backslash -1}$	2-36
2.3-5	Altitude Dependence of the Species Number Density Normal Profiles, $s_b/R_N = 6.125^{\backslash 1}$	2-37
2.3-6	Altitude Dependence of the Species Number Density Normal Profiles; $s_b/R_N = 2.433^{\backslash 2}$	2-39

SECTION 1
INTRODUCTION

The study under which this report is written covers two main theoretical disciplines: fluid mechanics and electromagnetic wave propagation in plasmas. Generally speaking, when theoretical calculations are to be performed, it is necessary to obtain the fluid mechanic effects upon which the reentry plasma properties depend before proceeding to the electromagnetic propagation analysis. The scope of work in both areas covers literature reviews as well as parametric calculations. But in order to allow lead time to the propagation calculations, the parametric flow field evaluation was begun immediately. The final report will cover the fluid mechanic state of the art evaluation. This report covers the results of inviscid flow field calculations by the streamtube method, which is described in detail below.

The problem of the propagation of signals from a radio wave source aboard a vehicle re-entering the atmosphere at hypersonic speeds involves many areas of electromagnetic theory and plasma physics. Antennas must be considered in terms of electrical characteristics and near field distributions. The linear effects of interaction of the antenna with the reentry plasma must be considered with respect to antenna impedance and pattern distortion.

Antenna breakdown is an important consideration, especially at high transmitted power levels. This problem must first be considered in the static environment of undisturbed cool air. Then the effects of reentry, where experimental data are much less plentiful, must be considered. Hopefully an extension of the well substantiated theory for the static environment can be carried out in such a way as to cover reentry effects.

Nonlinear propagation effects must be considered in terms of attenuation and distortion as functions of input power level. Finally, the possible techniques of alleviating all of the above effects must be evaluated. All of these areas of antennas and propagation are summarized in the following sections in terms of the significant literature.

SECTION 2

FLOW FIELD ANALYSIS

Typical results from the inviscid flow fields which have been generated as inputs to the parametric study of the electromagnetic wave propagation problems are presented and briefly discussed. In both the selection of these results and the accompanying discussions, emphasis has been placed on the nose bluntness and altitude effects on the nonequilibrium flow properties, and particular attention has been directed toward the contrast between chemical equilibrium and nonequilibrium effects.

The discussion which follows has been divided into four parts. Described in Section 2.1 is the steady inviscid thermochemical equilibrium flow field solution which has been used to provide the basis for all of the inviscid plasma work done for this report. Section 2.2 describes the thermal equilibrium multicomponent chemically reacting streamtube solution which has been used in conjunction with the equilibrium flow field solution to obtain the nonequilibrium flow properties. In Section 2.3 the results, presented in Figures 2.3-1 through 2.3-26 are discussed. In Section 2.4, future flow field work is discussed.

2.1 EQUILIBRIUM INVISCID FLOW FIELD SOLUTION

The inviscid thermochemical equilibrium flow fields that have been produced for this study were obtained from the direct detached shock solution of Gravalos, Edelfelt and Emmons [1*] in the transonic region, and by the method of characteristics solution of Jones and Friedhofer[2] as modified by Edsall[3], in the supersonic region. In the transonic region, the solution is obtained in intrinsic coordinates (streamwise - normal coordinates) by a forward-marching finite-difference integration along normals. In practice, the direct transonic solution is obtained by prescribing the body geometry, the free stream conditions and initial estimates of the body surface pressure distribution and shock shape, solving the governing equations as described above and, then, based on the results, modifying the surface pressure distribution

*References appear in Section 5.

and shock shape, and iterating until the boundary conditions at the shock are satisfied to within a specified tolerance. After this solution has been determined, the results at the downstream end of the transonic region provide the necessary initial data for the characteristics solution. In both regions the thermochemical equilibrium properties of air are treated by defining what is known as a "γ^* gas" according to the relation:

$$\left(\frac{\partial P}{\partial \rho}\right)_S = \gamma^* \frac{P}{\rho} \qquad (2.1\text{-}1)$$

in which P signifies the static pressure, ρ the static density, S the entropy and γ^* is determined by curve fits of the data taken from the NBS tables [4] in the form:

$$\gamma^* = \frac{a}{P} + b \qquad (2.1\text{-}2)$$

where a and b are continuous functions of entropy and piecewise continuous functions of pressure. Although the γ^* gas is an approximation to real equilibrium air, its validity as well as the validity of the methods of solution have been substantiated by comparisons with other solutions and with experimental data.

2.2 NONEQUILIBRIUM STREAMTUBE SOLUTION

The inviscid thermal equilibrium, chemical nonequilibrium results produced for this study were obtained from the streamtube solution of McMenamin and O'Brien[5]. In essence, the nonequilibrium streamtube method consists of the finite-difference simultaneous solution of the governing equations for the steady inviscid flow of a reacting multicomponent gas in intrinsic coordinates by deleting the transverse momentum equation(s) and independently prescribing the streamwise variation of one of the flow properties. It should be understood that the streamtube method is approximate only to the extent that the prescribed streamwise governing variable is approximate, but that to prescribe the streamwise governing variable exactly would require the exact nonequilibrium multidimensional flow field solution to be known. The usefulness of the streamtube method, therefore, derives from the fact that for

shock layer flows the static pressure is relatively insensitive to nonequilibrium effects, a result which can be ascertained by comparing the pressure fields for the two limiting cases of frozen and equilibrium flows. Consequently, by applying the nonequilibrium streamtube analysis to a sufficient number of streamlines from either an equilibrium or a chemically frozen flow field, a good approximation of the nonequilibrium flow field can be obtained. Indeed, when the streamtube method is judiciously applied, the results can be exceptionally good. In detached shock layer flows the predominant nonequilibrium effect on the shock is to increase the shock detachment distance (by as much as a factor of 2-1/2) over the corresponding equilibrium value. To a lesser degree the shock shape in the nose region is more blunt, for the nonequilibrium case than it is for the corresponding equilibrium case. When these two effects are taken into account and the pressure that is obtained from the thermal equilibrium frozen shock flow solution is used to replace the equilibrium pressure behind the shock, the exact boundary conditions for the nonequilibrium flow field can be approximated quite closely and, consequently, the streamwise pressure distribution used with the streamtube solution can be adjusted even closer to the exact nonequilibrium pressure distribution than if it were taken directly from the equilibrium flow field.

As pointed out in Reference 5, the validity of the nonequilibrium streamtube solution has been substantiated by comparisons with experimental data and with exact numerical flow field solutions for the following cases:

a. In a comparison with the shock tube electron density measurements of Lin, Neal, and Fyfe[6], the results of the steamtube solution were within the maximum estimated error of the data (±50%).

b. In a comparison with the shock layer electron density measurements of Kaegi and Chin[7], the results of the streamtube solution were within the interpretation of the data in the inviscid region.

c. In a comparison with the nonequilibrium method of characteristics solution of Gravalos and Studerus[8] for the properties along a cone surface, the streamtube results were in virtually exact agreement.

Also, it is of interest to note that in the electron density sensitivity study for sphere-cone streamtube applications, which was reported in Reference 5, it was determined that for a constant difference of $\pm 10\%$ in the streamwise pressure distribution (which is representative of the largest error introduced by assuming an equilibrium pressure distribution) the electron density was affected by less than $\pm 50\%$.

2.3 RESULTS

The configuration selected for this study is an 8.6 degree sphere-cone with a nose radius of 0.5 inch. According to the method of solution discussed in Section 2.1, flow fields for this configuration were obtained at altitudes of 50, 100, 150, 200 and 250 kilofeet. The free stream conditions for each of these flow fields are listed in Table 2.3-1.* The first four of these flow fields were determined under the condition of chemical equilibrium, whereas at 250 kilofeet a perfect gas ($\gamma = 7/5$) flow field was obtained to serve the double purpose of providing steamwise pressure distributions needed in the nonequilibrium streamtube analysis for the plasma attenuation study, and also to provide the gas dynamic properties in the limiting case of no vibrational excitation which will be needed in the antenna breakdown analysis.

The reaction system used in the nonequilibrium streamtube solution along with the kinetic rate coefficients and the collision efficiencies is shown in Table 2.3-2. The nonequilibrium results which are presented in Figures 2.3-1 through 2.3-26 were obtained in the following manner. Using streamwise pressure distributions from the perfect gas or equilibrium flow fields for selected streamlines (which herein are identified by the bow shock angle at the streamline-bow shock intersection), the nonequilibrium streamtube solution, which is coded in Fortran IV and run on the IBM 7094, is obtained for one streamline at a time, and the flow

*In the interest of brevity, floating point numbers in Table 2.3-1 through 2.3-7 have been expressed by means of a slash (after and slightly above the last significant figure) followed by the power of 10. For example, the number 1.234×10^{-8} is written 1.234 \-8. In addition it is to be understood that for the columned numbers the same exponent also applies to any number below written without one.

Table 2.3-1. Free Stream Conditions

Altitude		Velocity		Mach	Pressure		Density		Temperature
kilofeet	kilometers	ft/sec	cm/sec	Number	Atm	Torr	Amagat	gm/CC	^{o}K
$5.0\backslash^{1}$	$1.524\backslash^{1}$	$1.920\backslash^{4}$	$5.852\backslash^{5}$	$1.979\backslash^{1}$	$1.151\backslash^{-1}$	$8.748\backslash^{1}$	$1.524\backslash^{-1}$	$1.867\backslash^{-4}$	$2.166\backslash^{2}$
$1.0\backslash^{2}$	3.048	2.150	6.553	2.165	$1.100\backslash^{-2}$	$8.357\backslash^{0}$	$1.390\backslash^{-2}$	$1.703\backslash^{-5}$	2.270
1.5	4.572	2.195	6.690	2.042	$1.343\backslash^{-3}$	1.020	$1.448\backslash^{-3}$	$1.773\backslash^{-6}$	2.661
2.0	6.096	2.200	6.706	2.095	$1.954\backslash^{-4}$	$1.485\backslash^{-1}$	$2.208\backslash^{-4}$	$2.704\backslash^{-7}$	2.539
2.5	7.620	2.210	6.736	2.398	$2.007\backslash^{-5}$	$1.525\backslash^{-2}$	$2.946\backslash^{-5}$	$3.609\backslash^{-8}$	2.955

Table 2.3-2. Reaction System

Number		
1	$O_2 + M$	$O + O + M$
2	$N_2 + M$	$N + N + M$
3	$NO + M$	$N + O + M$
4	$NO + O$	$O_2 + N$
5	$N_2 + O$	$NO + N$
6	$N + O$	$NO^+ + e^-$

NOTE $M = O_2, N_2, N, O, NO$

Reaction Rate Constants, $k_{f,r} = A_{f,r} T^{B_{f,r}} \exp -(C_{f,r}/RT)$

	A_f	A_r	B_f	B_r	C_f	C_r
1	$2.5\backslash^{16}$	$8.9\backslash^{14}$	-.5	-.44	117945	0
2	$2.0\backslash^{21}$	$1.91\backslash^{20}$	-1.5	-1.57	225014	0
3	$5.5\backslash^{20}$	$1.67\backslash^{20}$	-1.5	-1.52	150002	0
4	$3.2\backslash^{9}$	$2.67\backslash^{10}$	1.0	.92	39100	7042.5
5	$6.8\backslash^{13}$	$2.1\backslash^{13}$	0	-.04	75011.5	0
6	$6.4\backslash^{9}$	$7.0\backslash^{18}$	.5	-.9	64356.5	0

NOTE: Units are moles/cc, sec., ^{o}K, and cal/gmol

Third Body Efficiencies (Based on Argon = 1)

Reaction	O_2	N_2	N	O	NO
1	5	2	2	25	2
2	2	5	3	5	2
3	2	2	5	5	2

properties are stored at the intersections of the streamline with the specified body normals. After the last streamtube run is made, the position of each streamline along each normal is determined by continuity, using the nonequilibrium values for the density and velocity. By selecting a sufficient number of streamlines and body normals, the end result is a well defined nonequilibrium flow field which is approximate only to the extent to which the bow shock and the streamwise pressure distributions are approximate.

For the present results, no attempt was made to adjust the perfect gas or equilibrium shock shapes for nonequilibrium effects. However, the pressure immediately behind the bow shock was in every case replaced by the value obtained from the thermal equilibrium frozen shock flow solution. Although the shock shape was not adjusted, it is significant to note that after constructing the approximate nonequilibrium flow fields, a comparison showed that the maximum percent difference in the shock radius is -3.5% between the nonequilibrium and frozen values and +3% between the nonequilibrium and equilibrium values. In Table 2.3-3, along with a summary of the body geometry corresponding to three normals which have been selected to display the nose bluntness and altitude effects on the nonequilibrium flow properties, a comparison is presented of the shock radii at the intersections of the shock and the normals as determined by the different solutions. By far, the larger part of the error is due to the fact that the perfect gas and equilibrium flow field values for the shock detachment distance were not adjusted for nonequilibrium before being used with the streamtube solution. This, however, will not significantly affect the results even along the normal on the nose.

The altitude trends of the shock radius comparison in Table 2.3-3, particularly for the first normal, are significant and deserve further attention. It may be noted that at 50 kilofeet the values of the shock radius according to the equilibrium and nonequilibrium solutions agree to within 0.06%, which indicates that the flow is nearly in equilibrium. As the altitude increases, the nonequilibrium value for the shock radius becomes increasingly larger than the equilibrium value, indicating that the flow is becoming further out of equilibrium. The comparison at 250 kilofeet with the perfect gas value, however, shows that even at this altitude the flow is not frozen in the nose region.

Table 2.3-3. Summary of Geometric Variables for Selected Body Surface Normals

s_b/R_N	X/R_n Y=O	R_b/R_n	Altitude (kilofeet)	(Y_{sn}/R_n) noneq	(R_{sn}/R_n) eq or fr	(R_{sn}/R_n) noneq
$4.962\backslash^{-1}$	$1.206\backslash^{-1}$	$4.761\backslash^{-1}$	$5.000\backslash^{1}$	$8.529\backslash^{-2}$	$5.164\backslash^{-1}$	$5.167\backslash^{-1}$
			$1.000\backslash^{2}$	7.989	5.133	5.141
			1.500	8.596	5.106	5.170
			2.000	9.352	5.093	5.20[illegible]
			2.500	$1.103\backslash^{-1}$	5.459	5.286
$6.125\backslash^{1}$	$6.000\backslash^{1}$	$9.934\backslash^{0}$	$5.000\backslash^{1}$	$1.706\backslash^{0}$	$1.141\backslash^{1}$	$1.162\backslash^{1}$
			$1.000\backslash^{2}$	1.440	1.130	1.136
			1.500	1.625	1.134	1.154
			2.000	1.598	1.131	1.151
			2.500	1.492	1.132	1.121
$2.433\backslash^{2}$	$2.400\backslash^{2}$	$3.716\backslash^{1}$	$5.000\backslash^{1}$	$5.352\backslash^{0}$	$4.225\backslash^{1}$	$4.245\backslash^{1}$
			$1.000\backslash^{2}$	4.800	4.191	4.190
			1.500	5.140	4.206	4.224
			2.000	5.154	4.241	4.225
			2.500	4.606	4.181	4.171

In Figures 2. 3-1 through 2. 3-10 the contrast between chemical equilibrium and non-equilibrium effects at an altitude of 150 kilofeet is demonstrated by plotting the streamwise variation of the flow properties against the distance along the body surface for three streamlines which intersect the bow shock at angles of approximately 50, 70 and 89 degrees. In sequence, these plots show this variation for the pressure, temperature, density, velocity component parallel to the surface (all normalized by the corresponding free stream quantities), and the number densities of molecular oxygen, molecular nitrogen, atomic nitrogen, atomic oxygen, nitric oxide and electrons. Before proceeding to a brief discussion of some of the more interesting aspects of these results, it should be pointed out that, in Figure 2. 3-1, due to the positive normal pressure gradient in the nose region, the higher shock angle streamlines initially expand more rapidly; however, in the over-expansion region this trend is reversed prior to converging at the cone surface pressure value.

For the nonequilibrium results shown in Figures 2. 3-1 through 2. 3-10, it may be noted that the flow on the 89 degree streamline is almost in equilibrium at the first normal. This is caused by its passage through the near stagnation region. At this point oxygen is almost entirely dissociated. As the flow continues to expand over the nose, atomic oxygen freezes in the nonequilibrium case, whereas for equilibrium it begins to recombine. This single feature, more than any other, determines the nonequilibrium effects which are indicated in these results.

In Figures 2. 3-11 through 2. 3-25, nose bluntness and altitude effects on the nonequilibrium flow properties are shown by plotting the flow properties against shock layer thickness, with altitude as a parameter, for three selected normals located along the body surface at s_b/R_N equal to 0. 4962, 61. 25 and 243. 3. Sequentially in groups of three, the normal profiles are given for the pressure, temperature, density and velocity parallel to the surface (all normalized by the corresponding free stream quantity) and the electron number density. Profiles of the remaining species number densities are presented in Table 2. 3-4, 2. 3-5 and 2. 3-6 for the different altitudes at the selected normals. In Figure 2. 3-26 the integral of the electron density across the shock layer is plotted against the normalized coordinate along

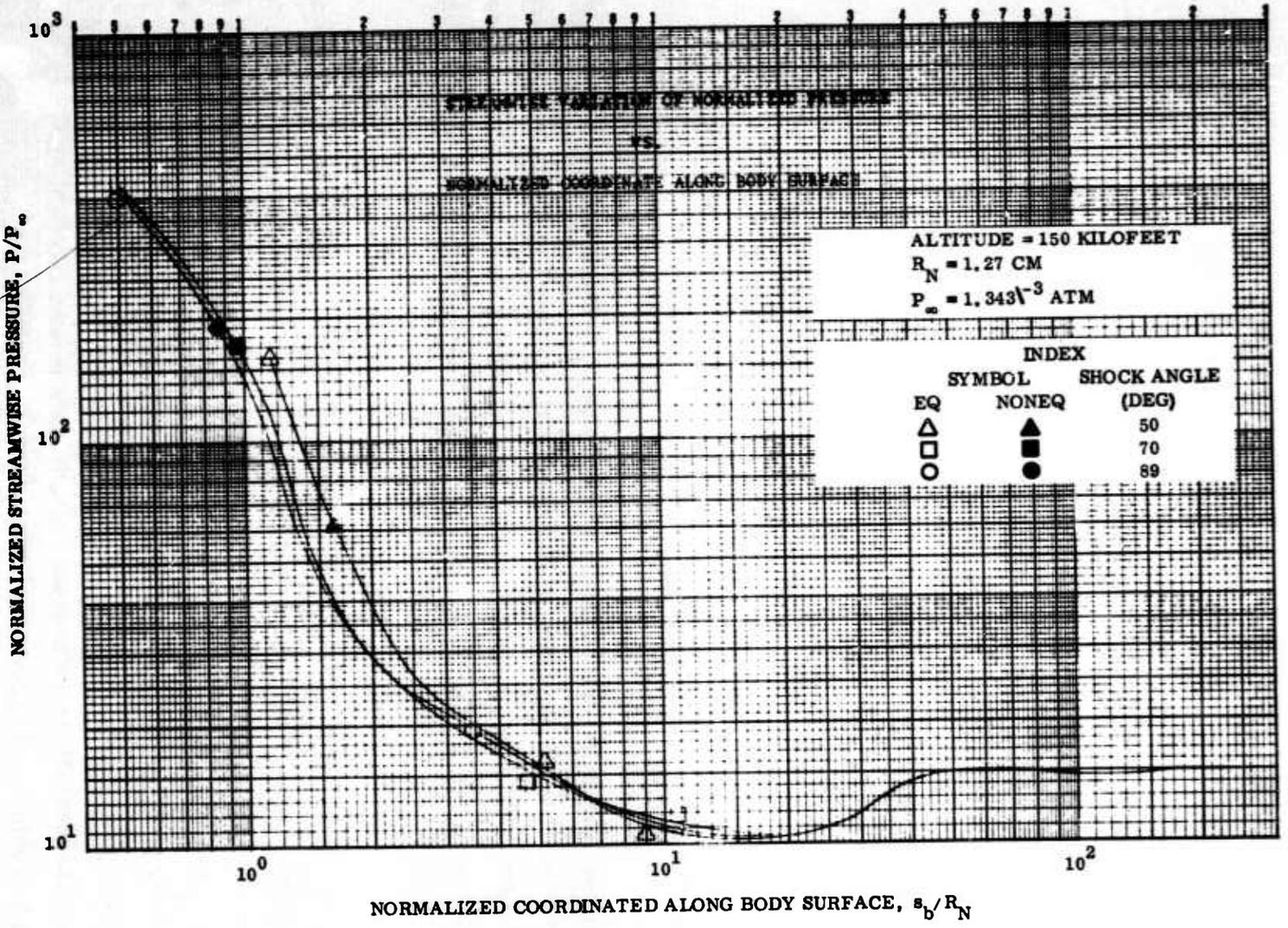

Figure 2.3-1. Streamwise Variation of Normalized Pressure vs Normalized Coordinate Along Body Surface

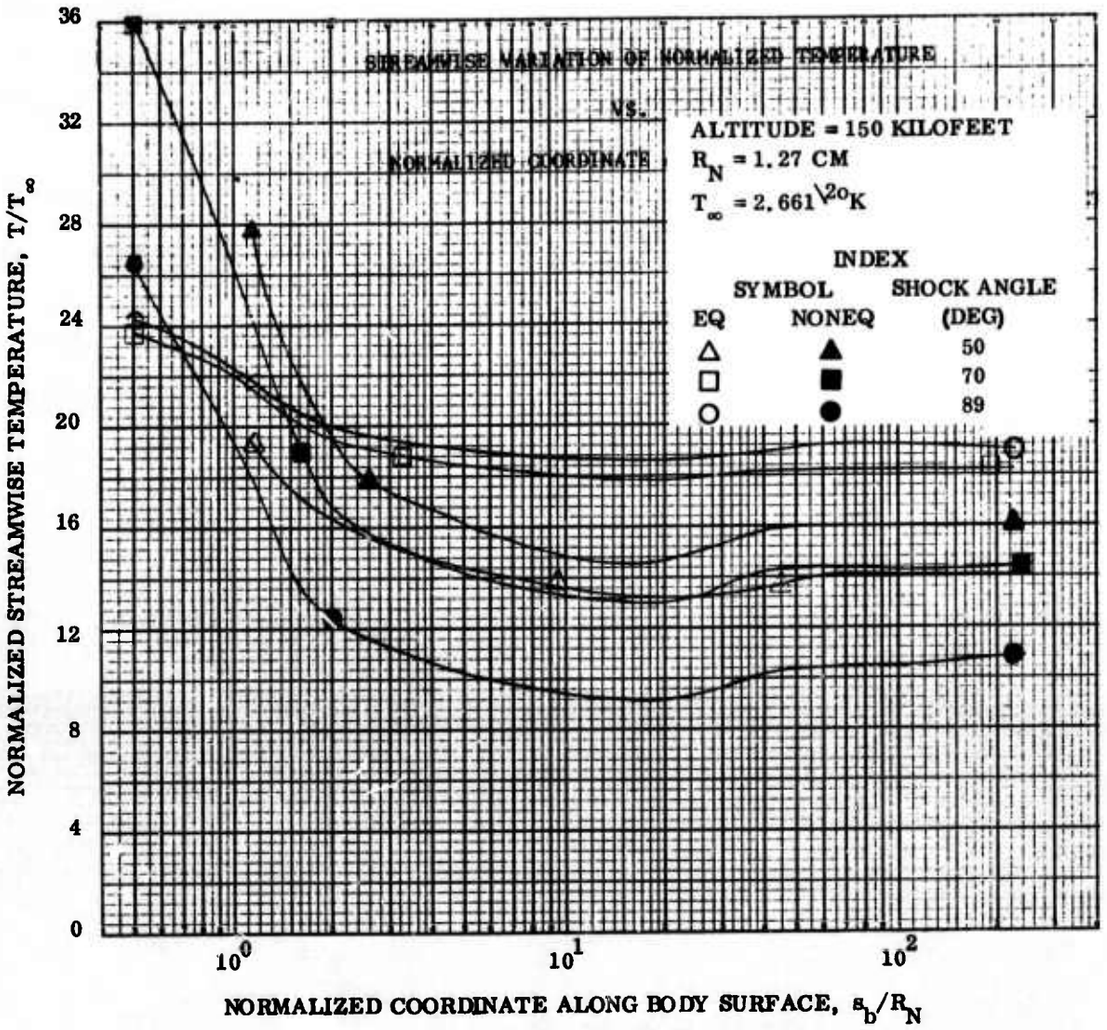

Figure 2. 3-2. Streamwise Variation of Normalized Temperature vs Normalized Coordinate Along Body Surface

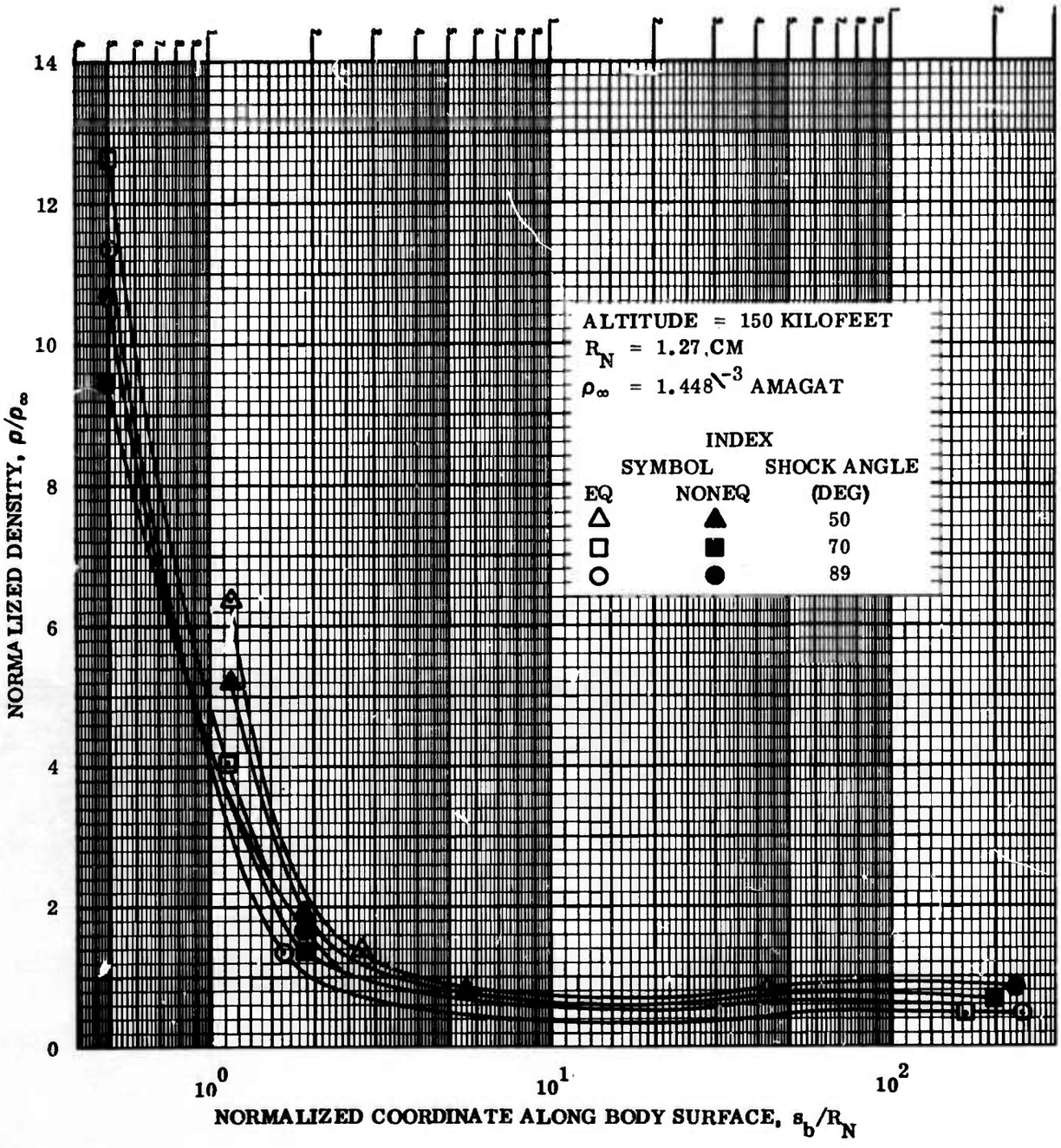

Figure 2.3-3. Streamwise Variation of Normalized Density vs Normalized Coordinate Along Body Surface

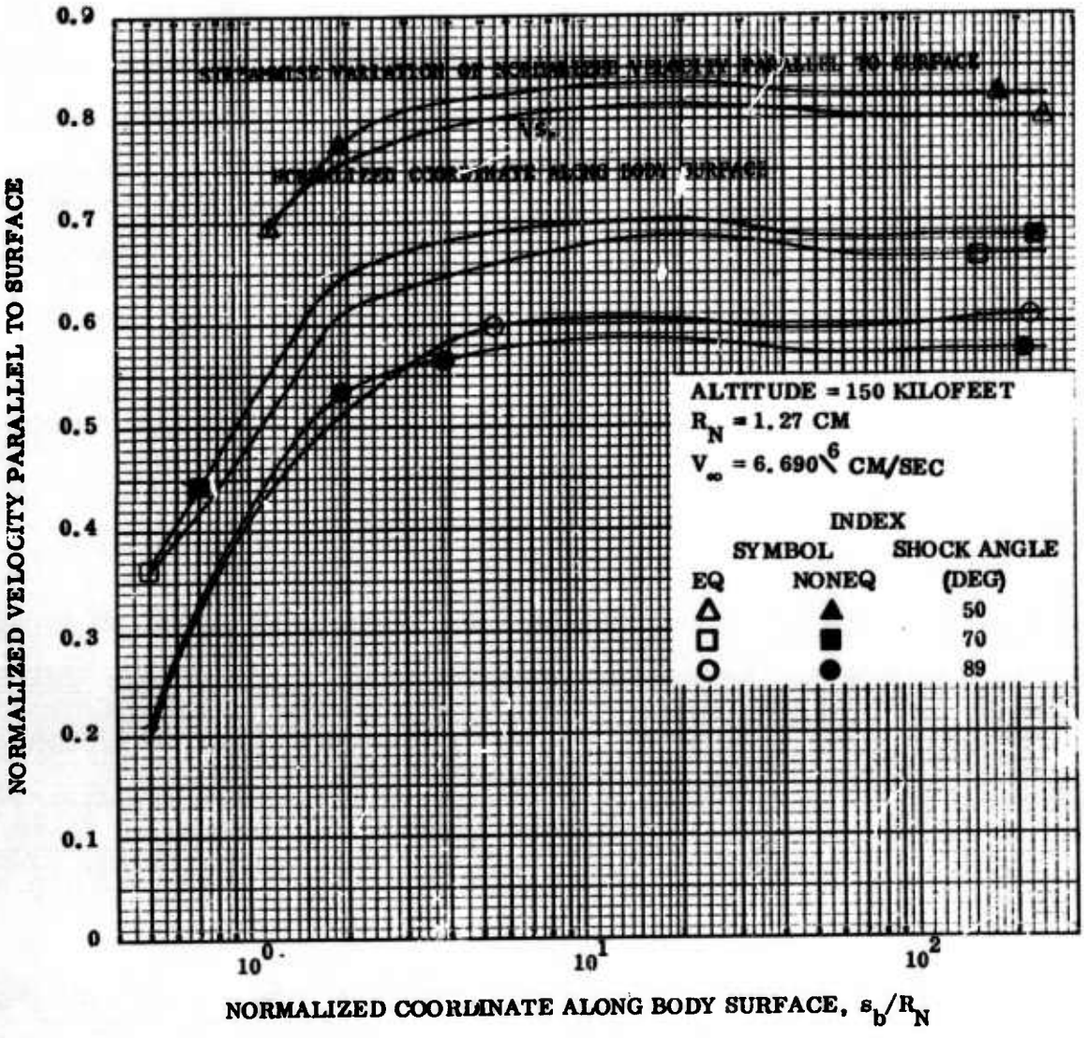

Figure 2. 3–4. Streamwise Variation of Normalized Velocity Parallel to Surface vs Normalized Coordinate Along Body Surface

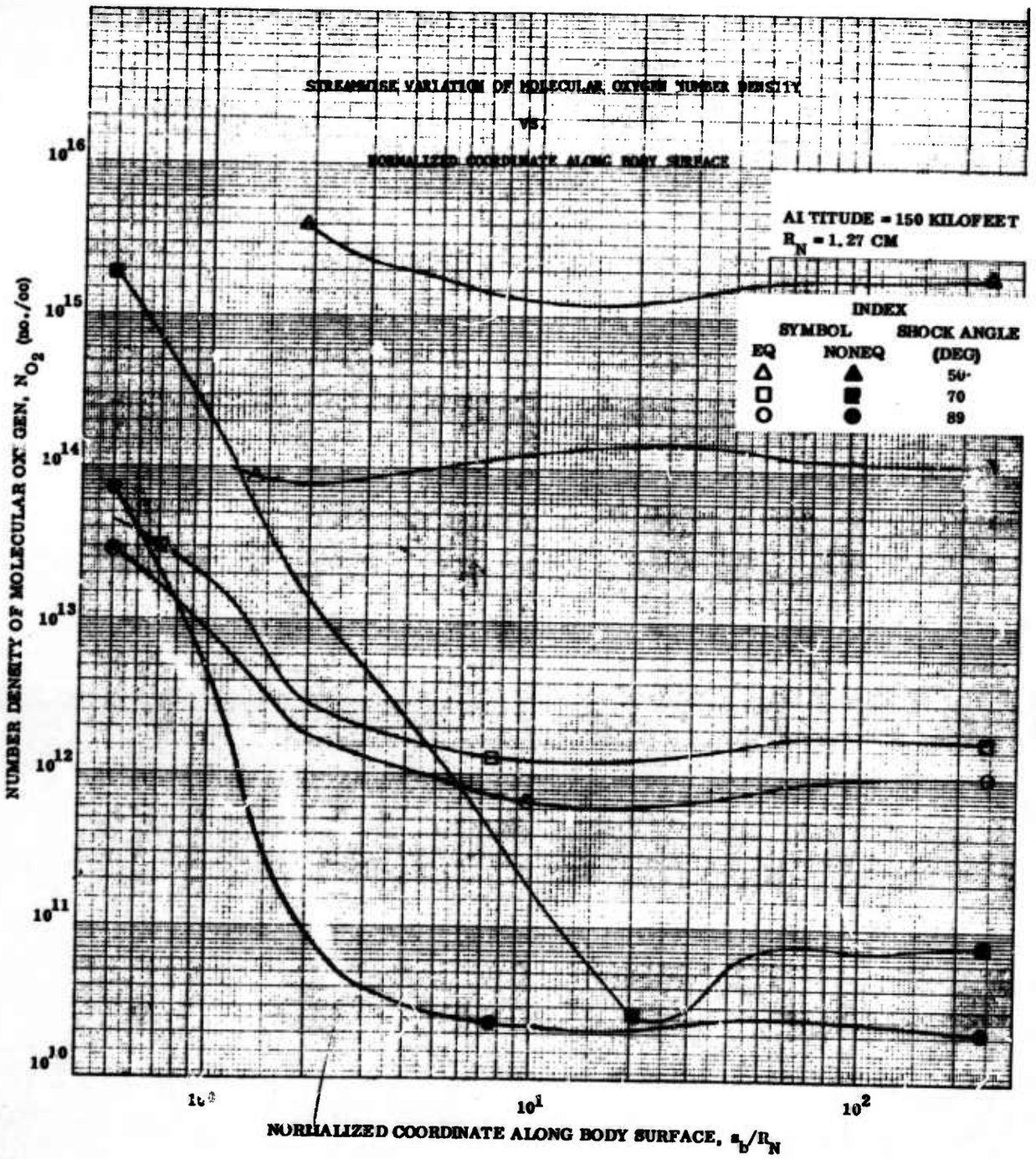

Figure 2. 3-5. Streamwise Variation of Molecular Oxygen Number Density vs Normalized Coordinate Along Body Surface

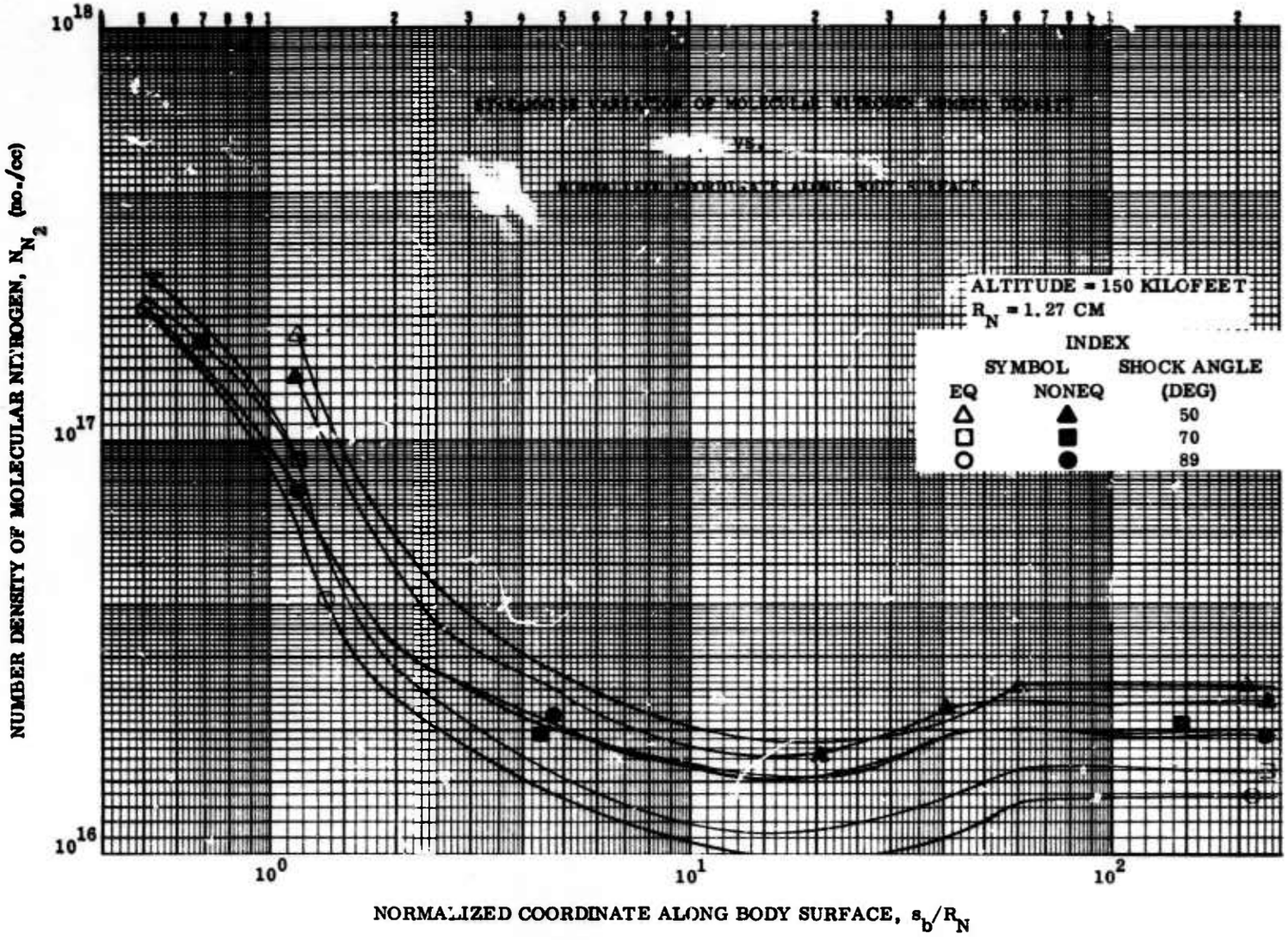

Figure 2.3-6. Streamwise Variation of Molecular Nitrogen Number Density vs Normalized Coordinate Along Body Surface

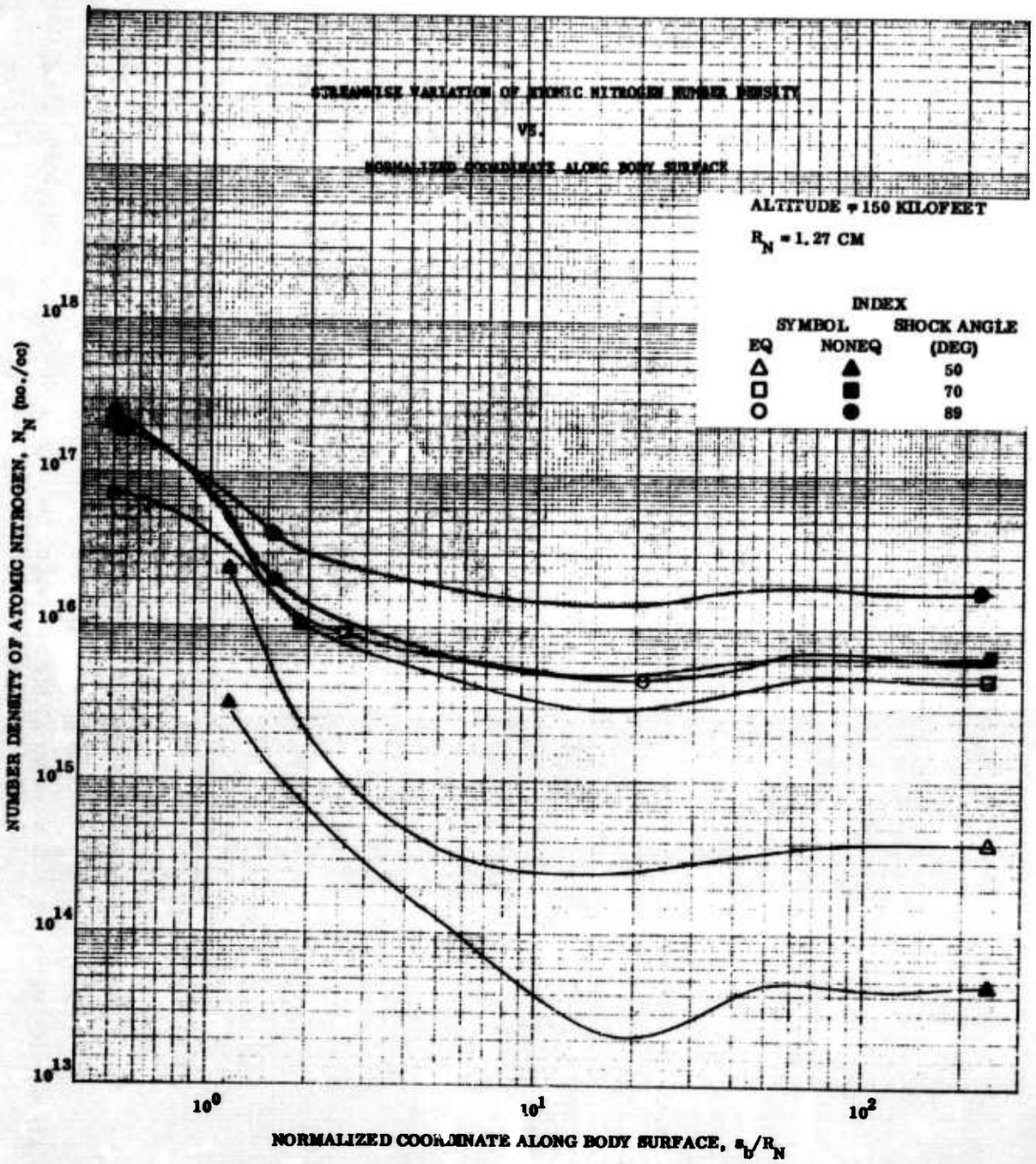

Figure 2.3-7. Streamwise Variation of Atomic Nitrogen Number Density vs Normalized Coordinate Along Body Surface

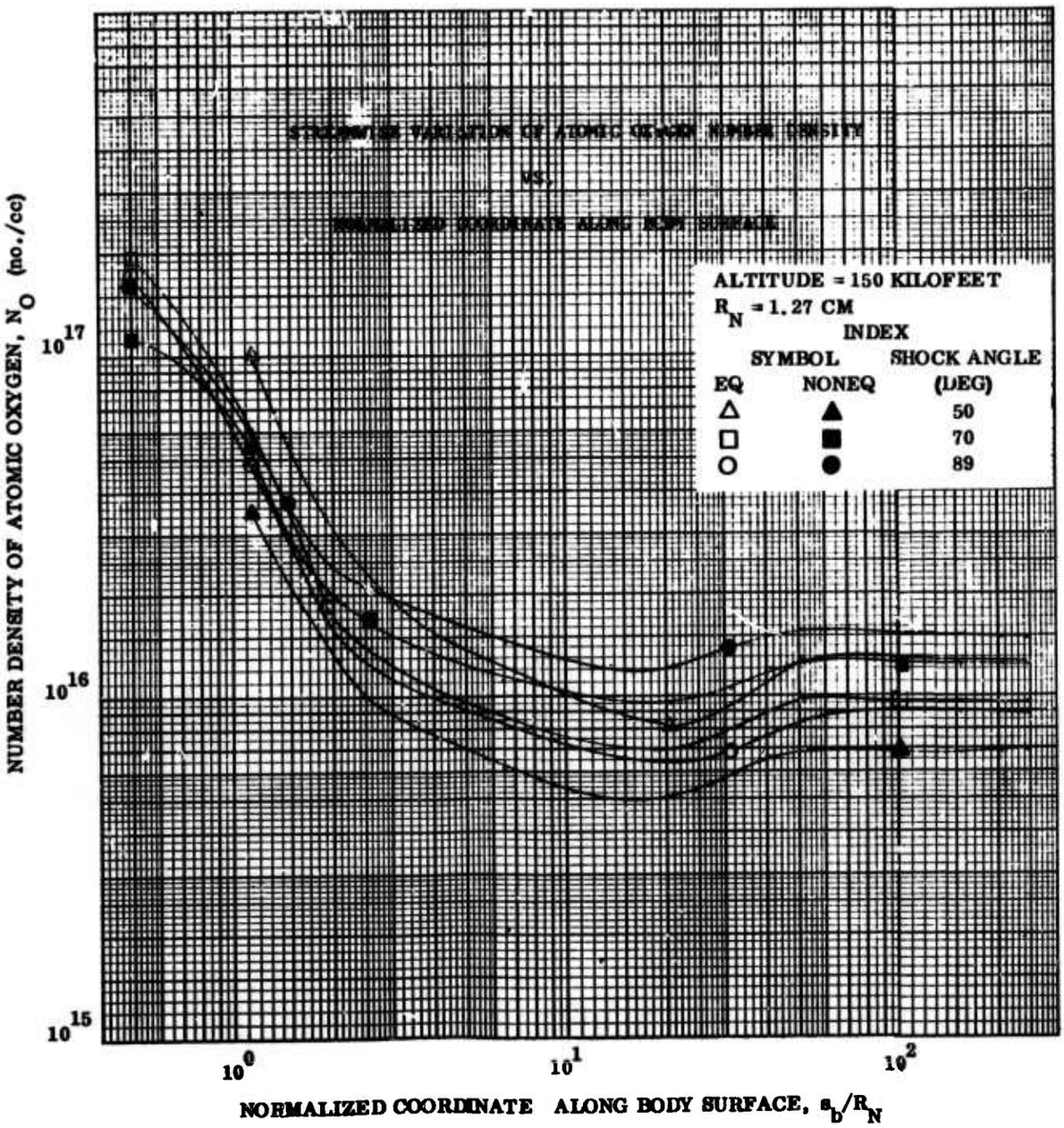

Figure 2. 3-8. Streamwise Variation of Atomic Oxygen Number Density vs Normalized Coordinate Along Body Surface

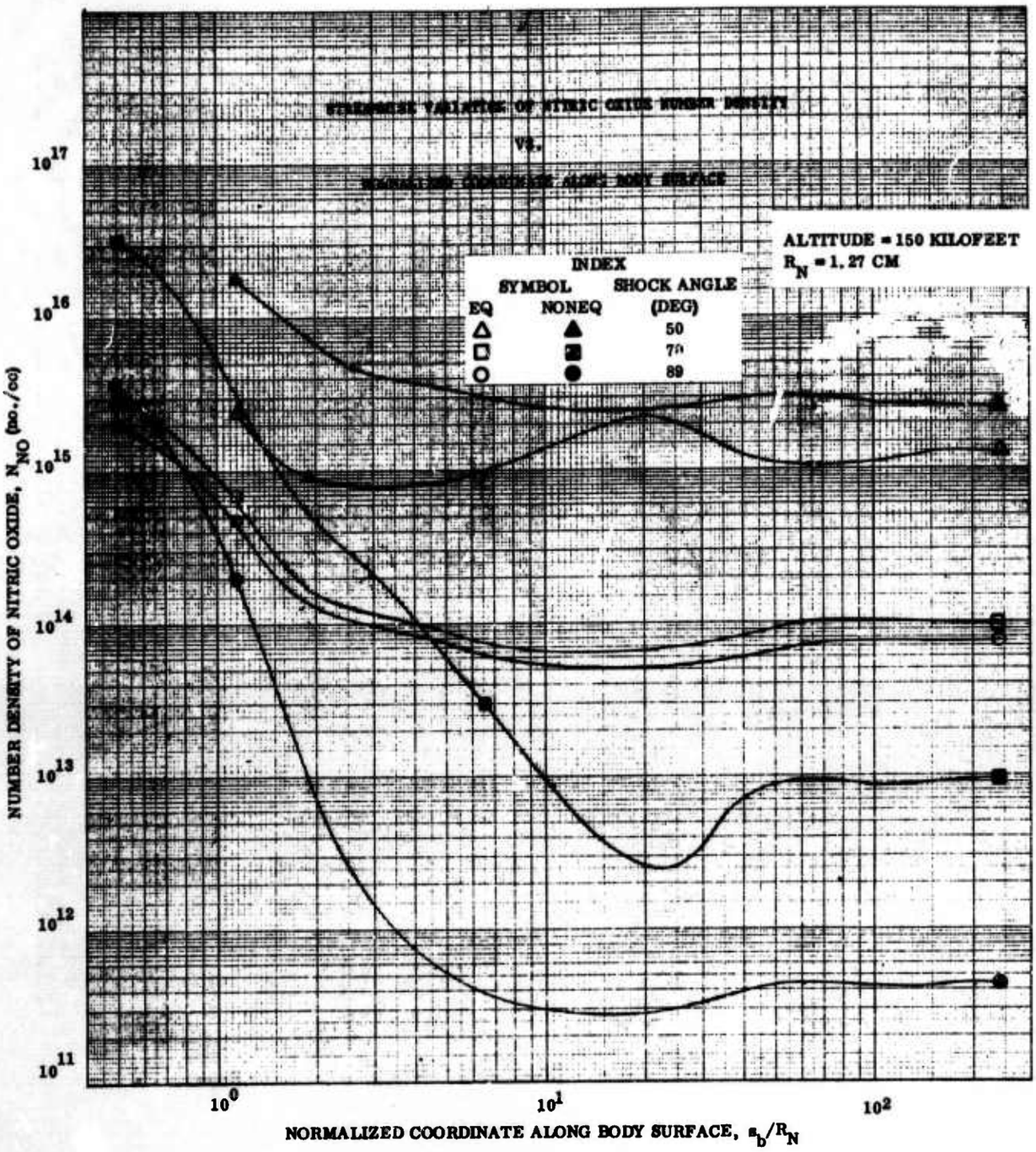

Figure 2.3-9. Streamwise Variation of Nitric Oxide Number Density vs Normalized Coordinate Along Body Surface

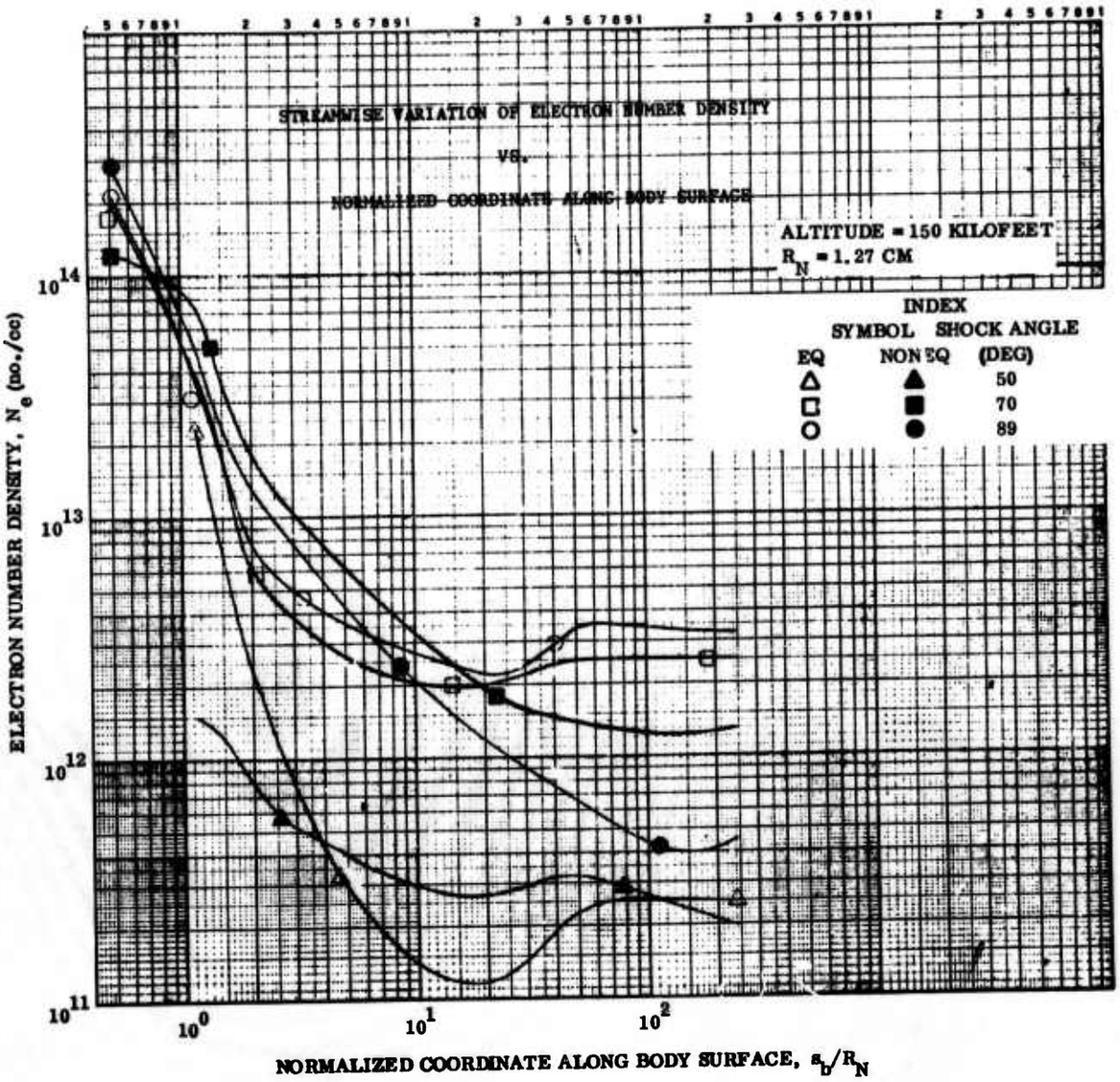

Figure 2. 3-10. Streamwise Variation of Electron Number Density vs Normalized Coordinate Along Body Surface

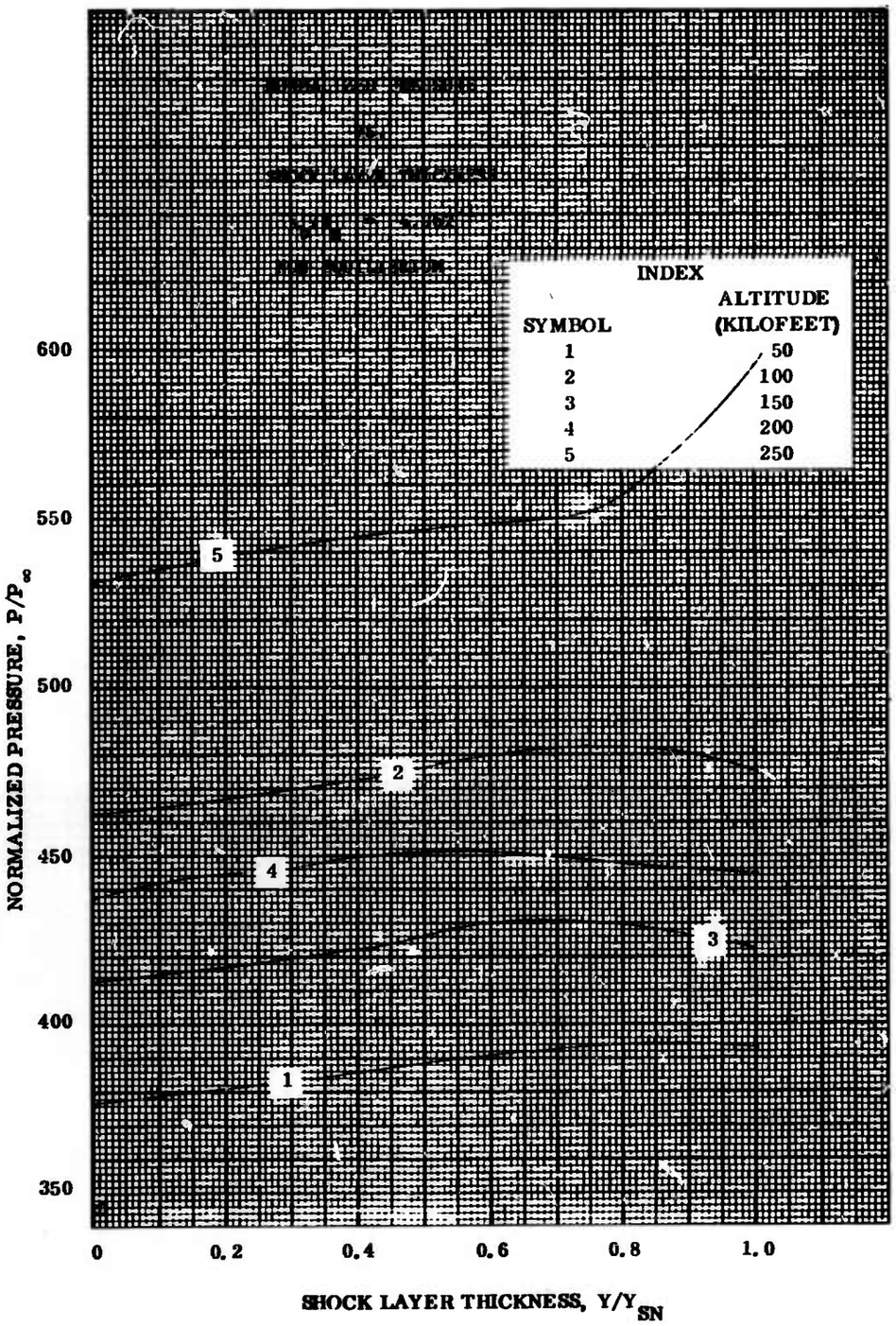

Figure 2.3-11. Normalized Pressure vs Shock Layer Thickness; $s_b/R_N = 4.962\backslash^1$; Nonequilibrium

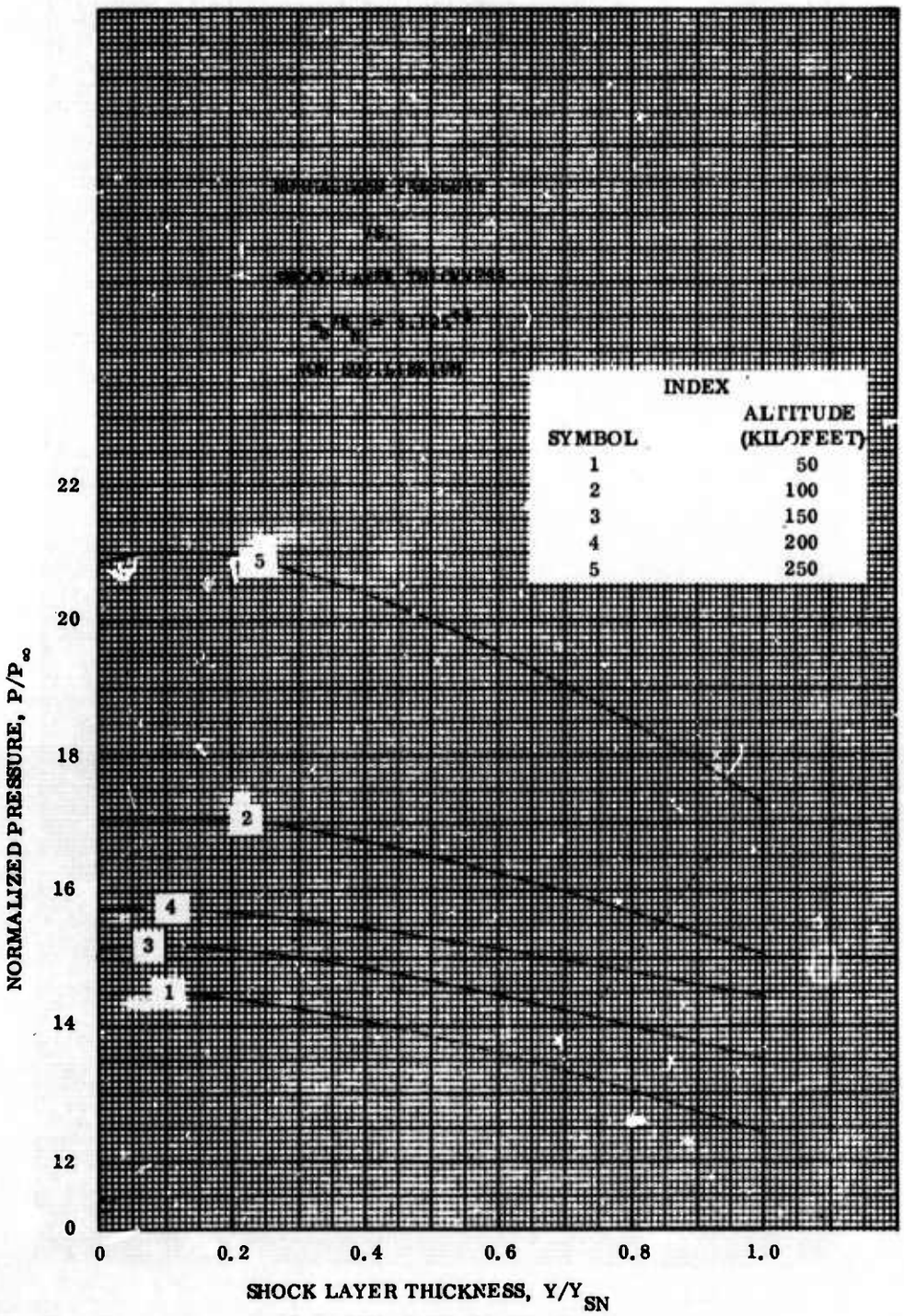

Figure 2.3-12. Normalized Pressure vs Shock Layer Thickness; $s_b/R_N = 6.125^{\backslash 1}$; Nonequilibrium

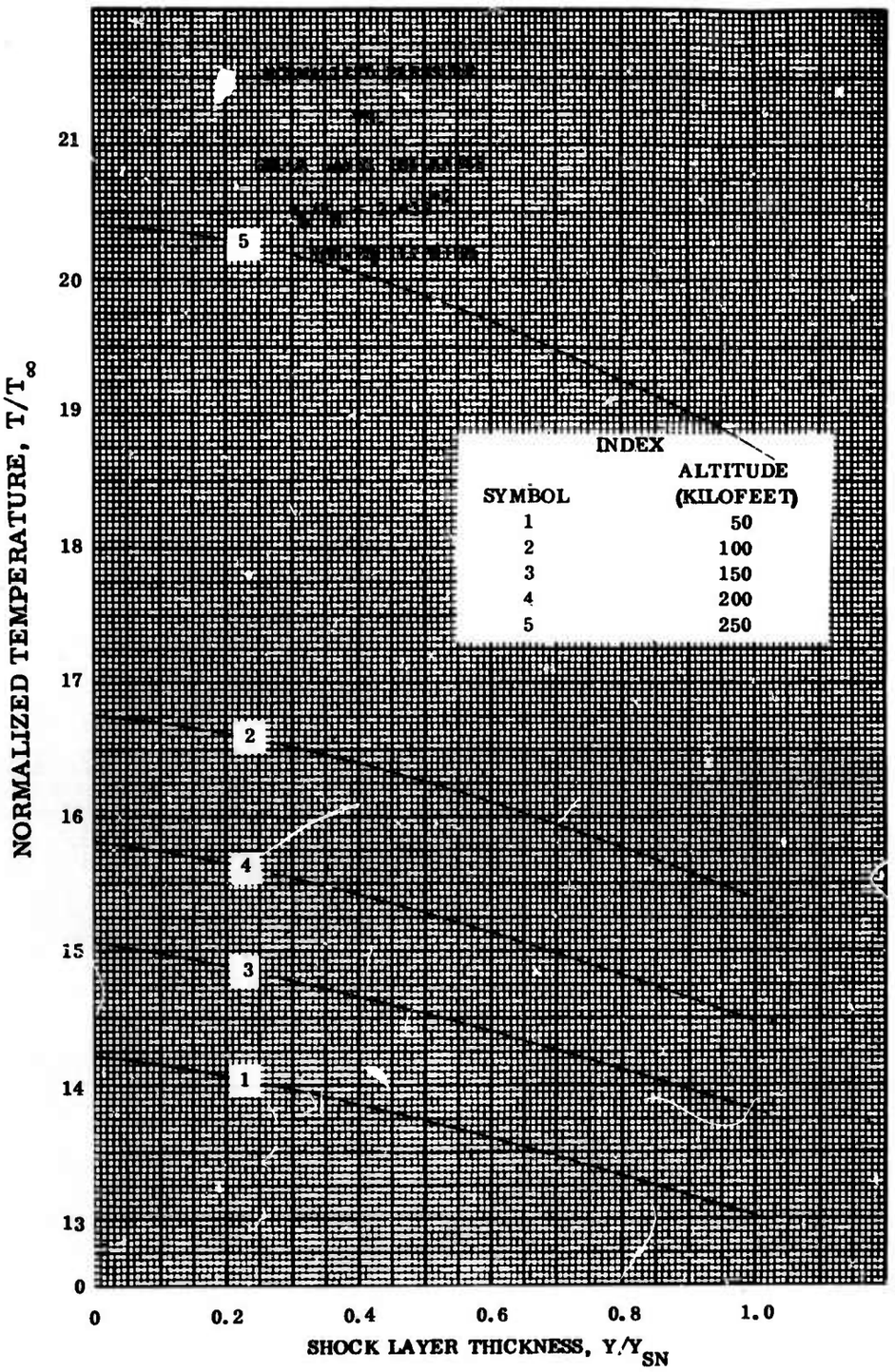

Figure 2.3-13. Normalized Pressure vs Shock Layer Thickness; $s_b/R_N = 2.433^{\backslash 2}$; Nonequilibrium

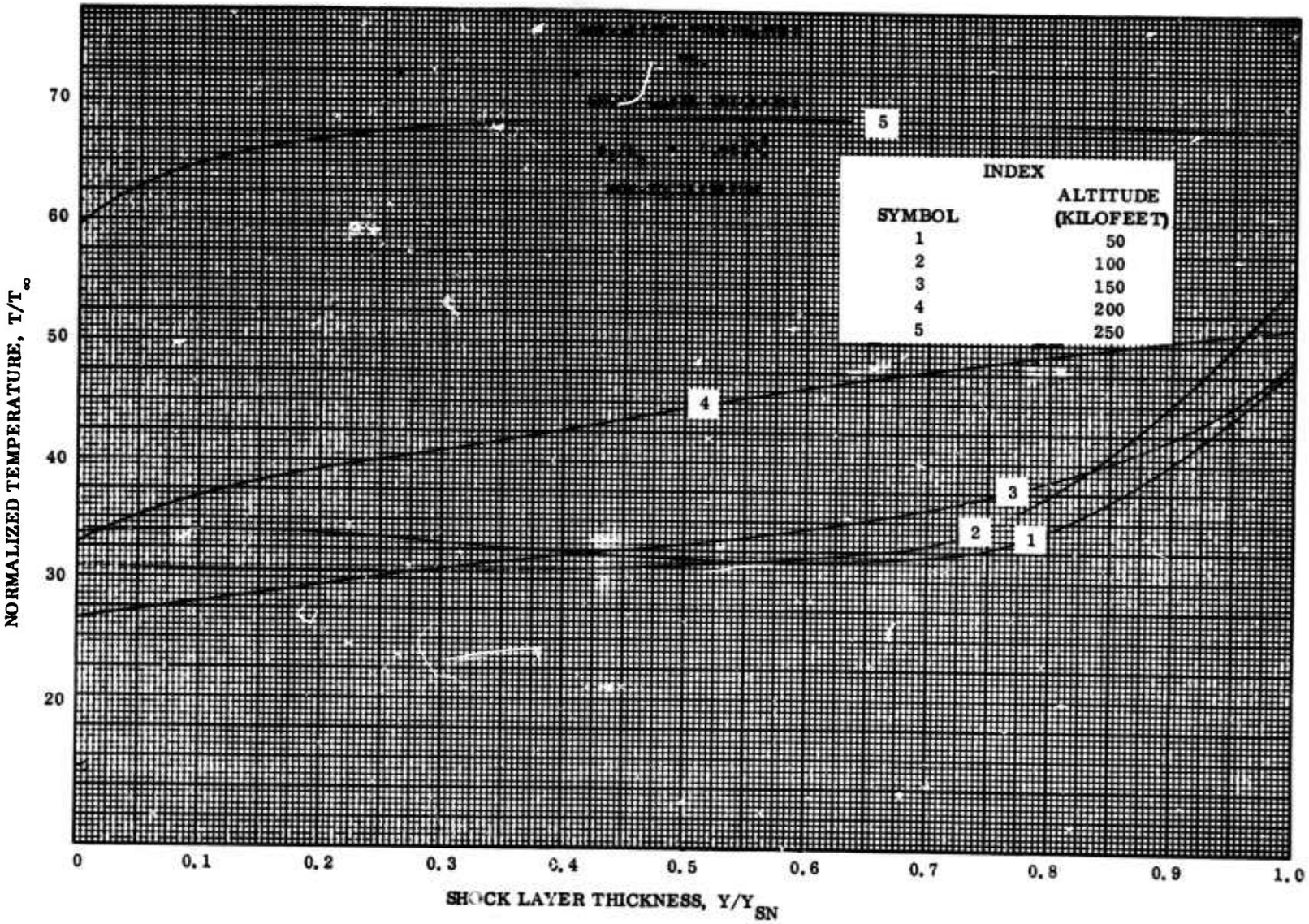

Figure 2.3-14. Normalized Temperature vs Shock Layer Thickness; $s_b/R_N = 4.962 \backslash^{-1}$; Nonequilibrium

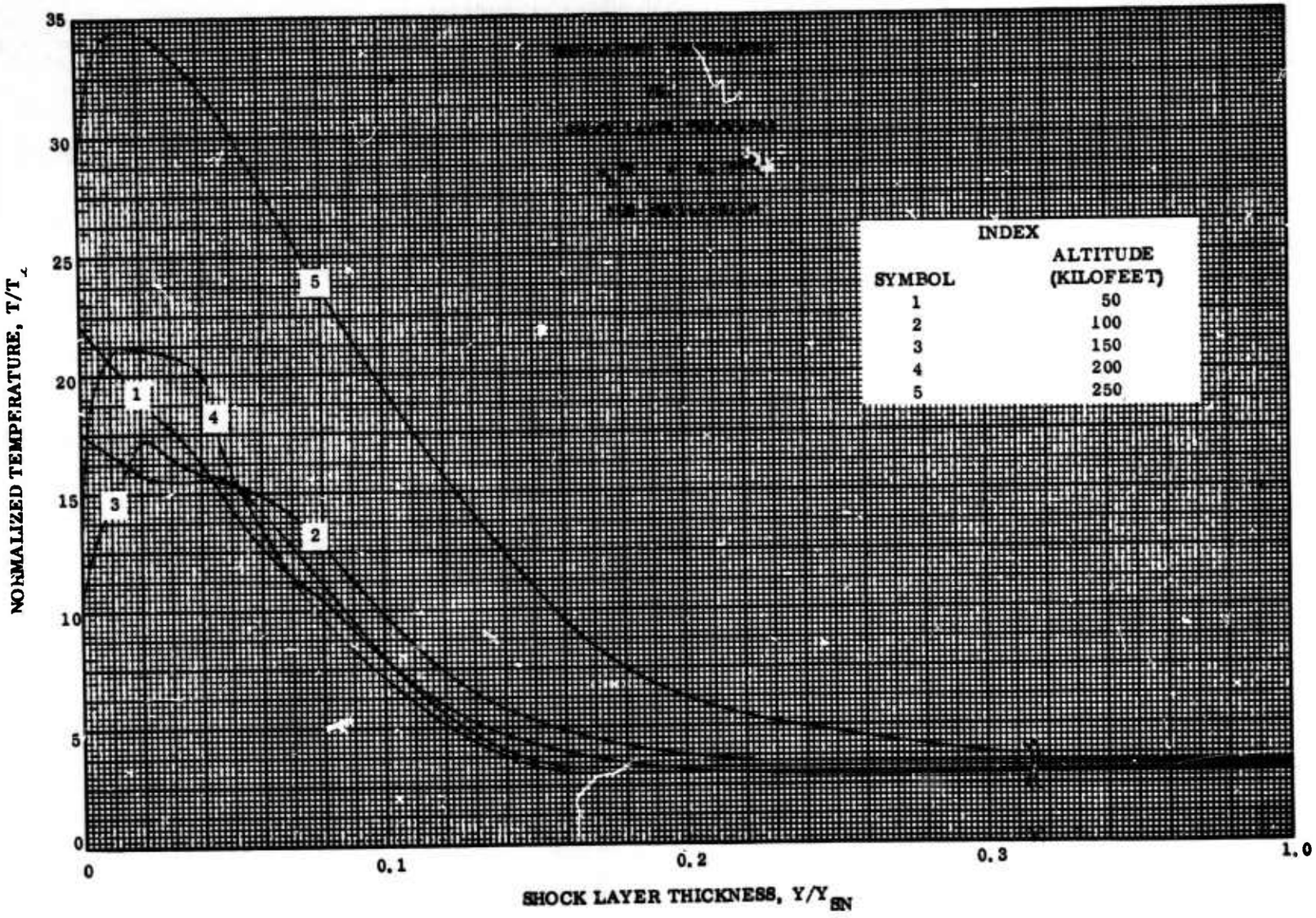

Figure 2.3-15. Normalized Temperature vs Shock Layer Thickness; $s_b/R_N = 6.125$ \1; Nonequilibrium

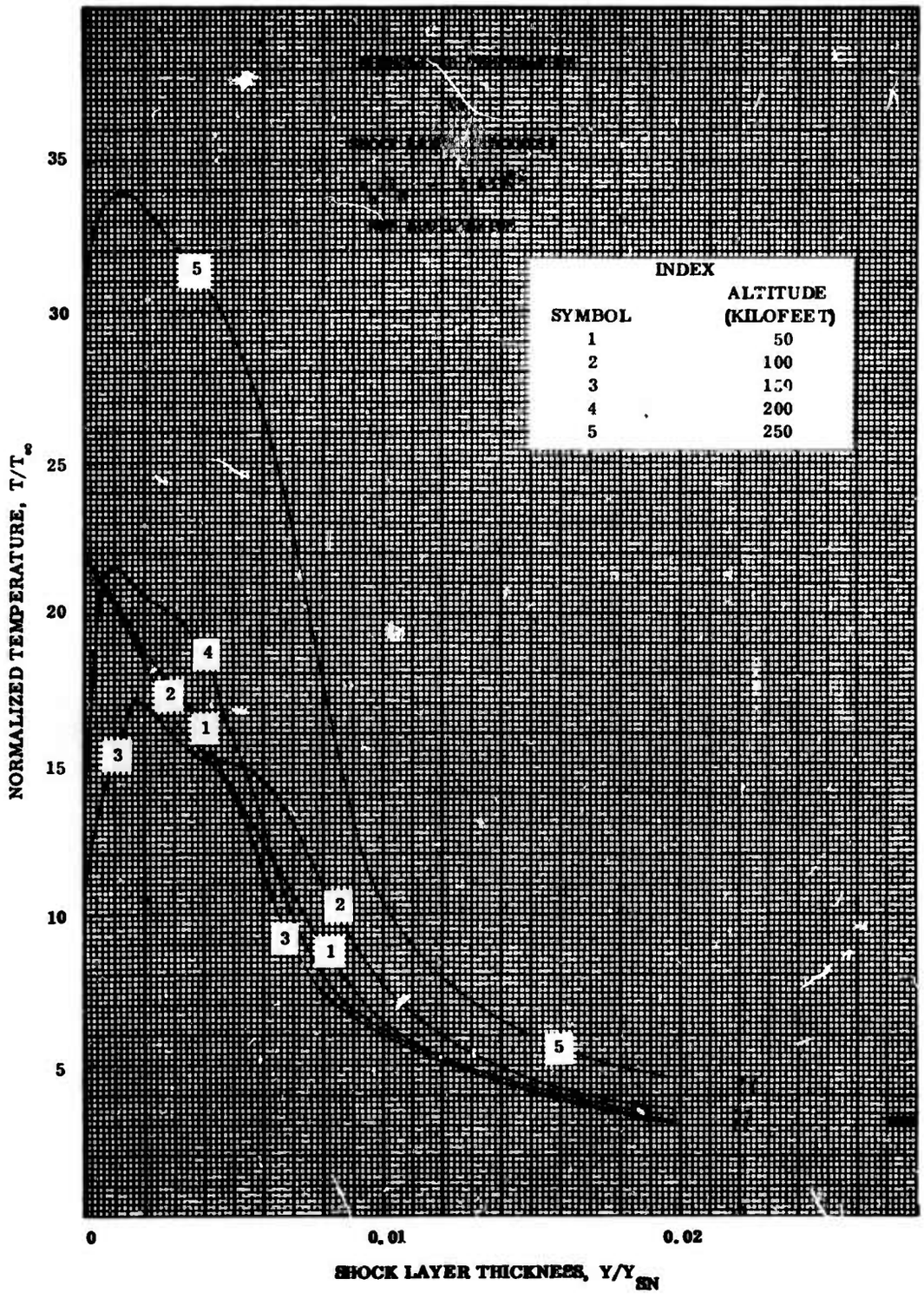

Figure 2.3-16. Normalized Temperature vs Shock Layer Thickness; $s_b/R_N = 2.433^{\backslash 2}$; Nonequilibrium

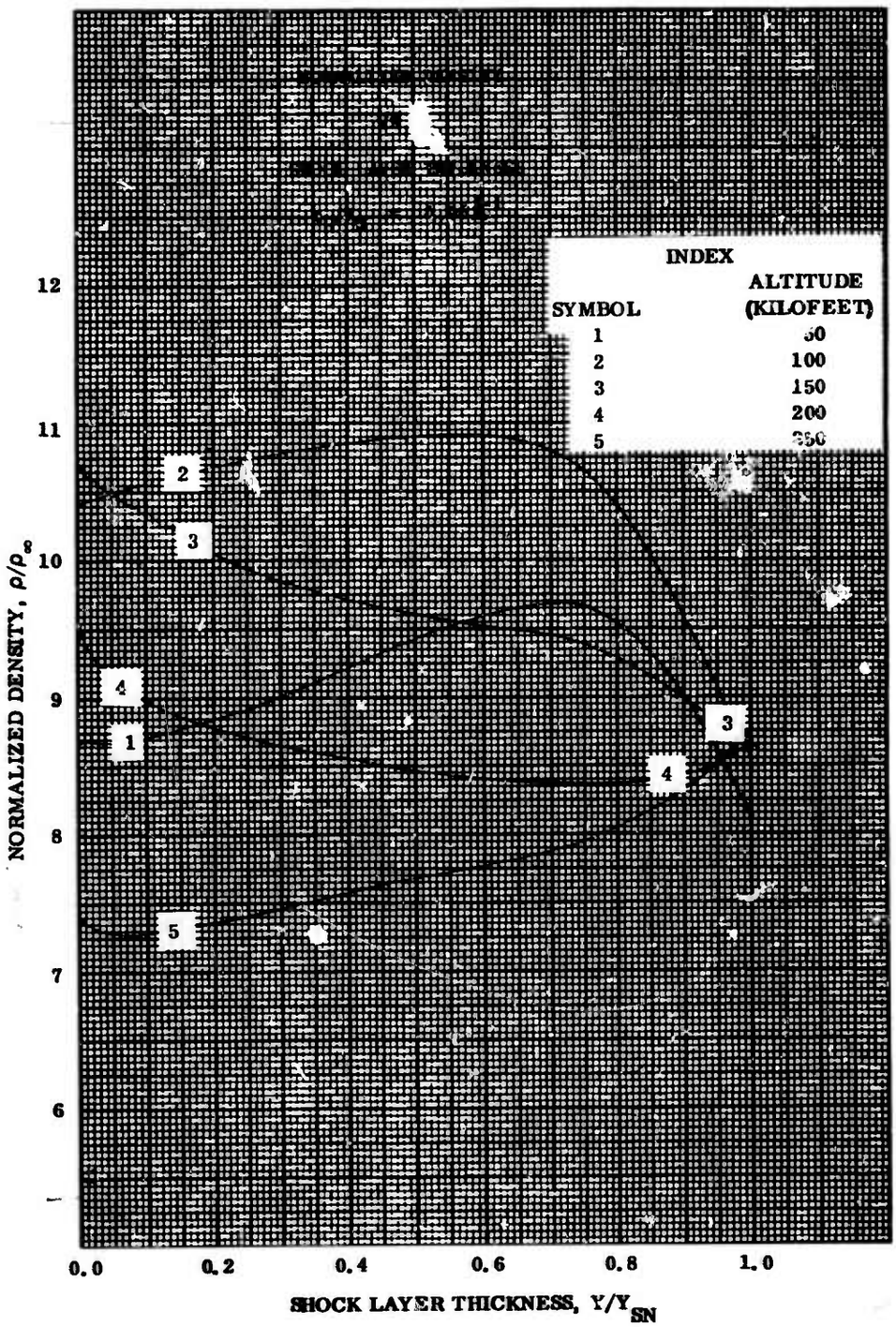

Figure 2.3-17. Normalized Density vs Shock Layer Thickness; $s_b/R_N = 4.962\backslash^{-1}$

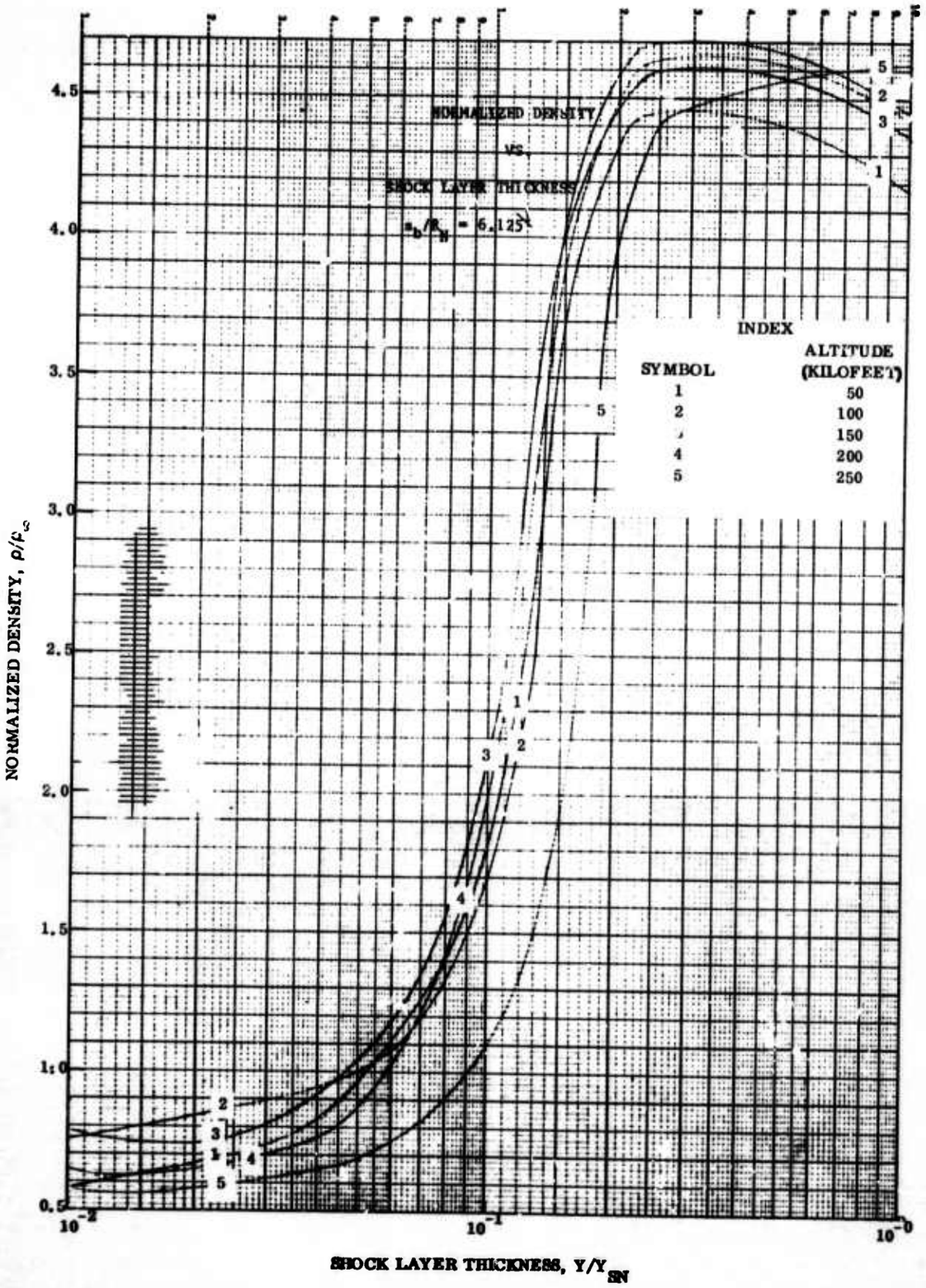

Figure 2.3-18. Normalized Density vs Shock Layer Thickness; $s_b/R_N = 6.125$

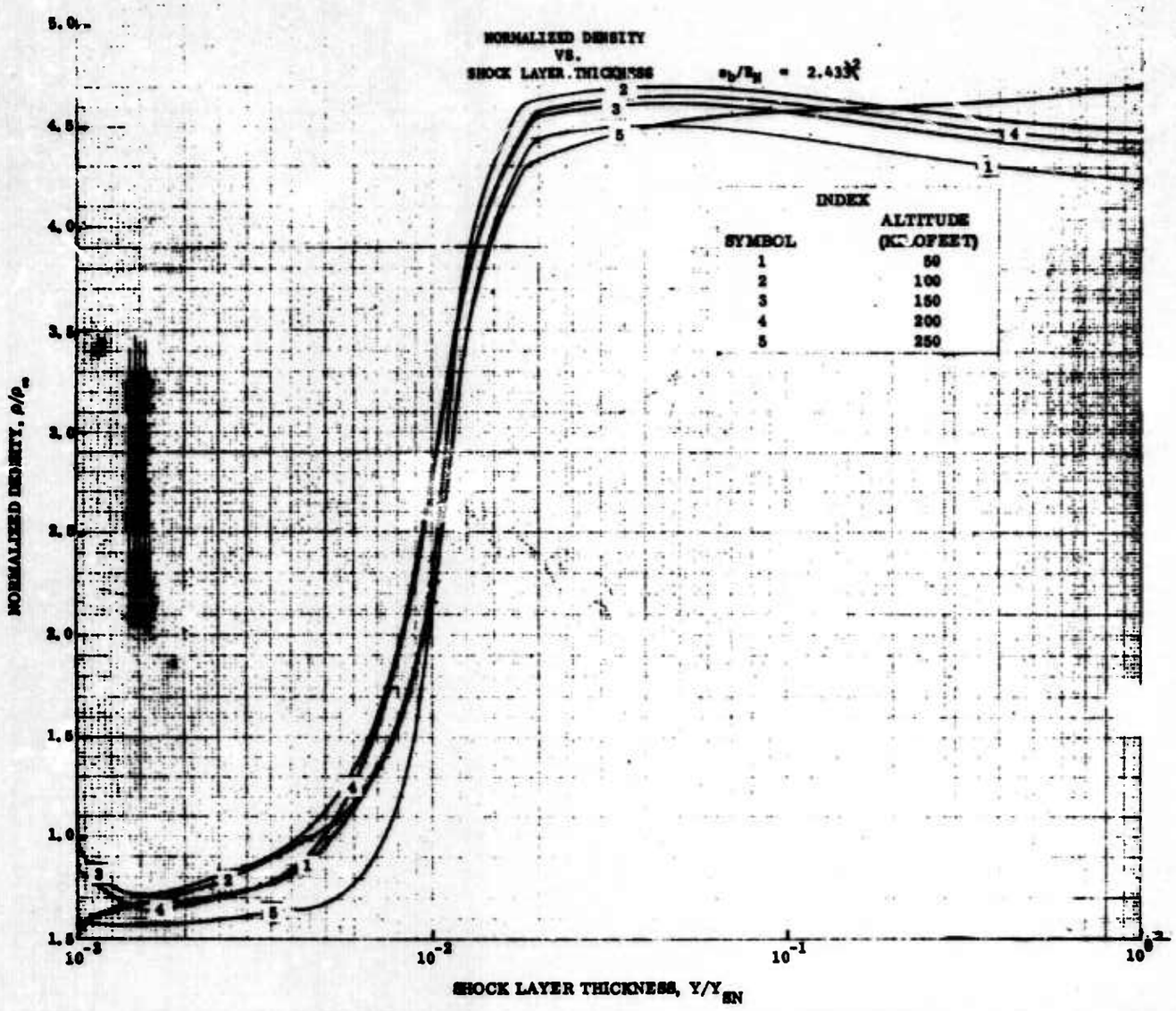

Figure 2.3-19. Normalized Density vs Shock Layer Thickness; $s_b/R_N = 2.433^2$

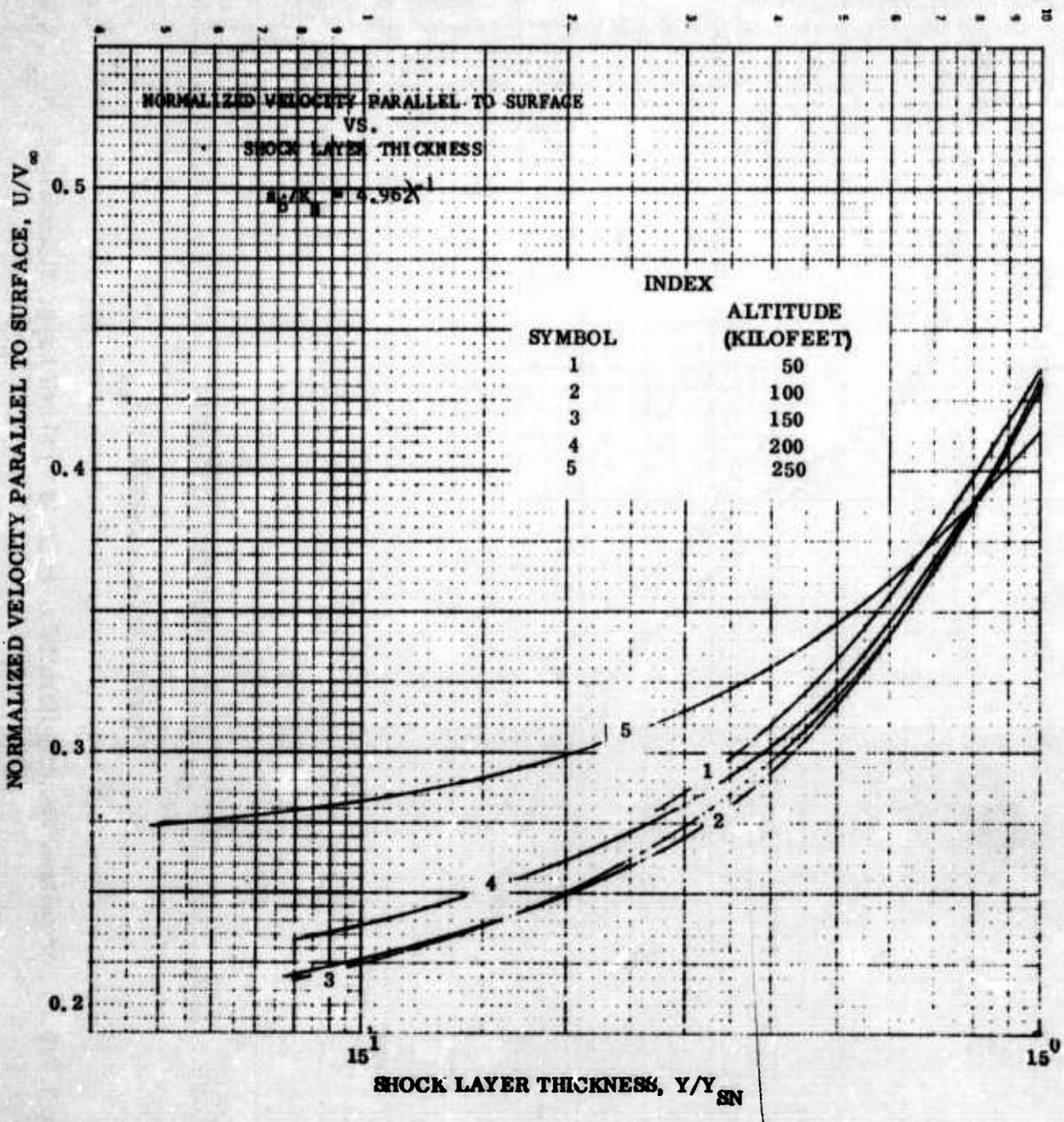

Figure 2. 3-20. Normalized Velocity Parallel to Surface vs Shock Layer Thickness; $s_b/R_N = 4.962^{\lambda-1}$

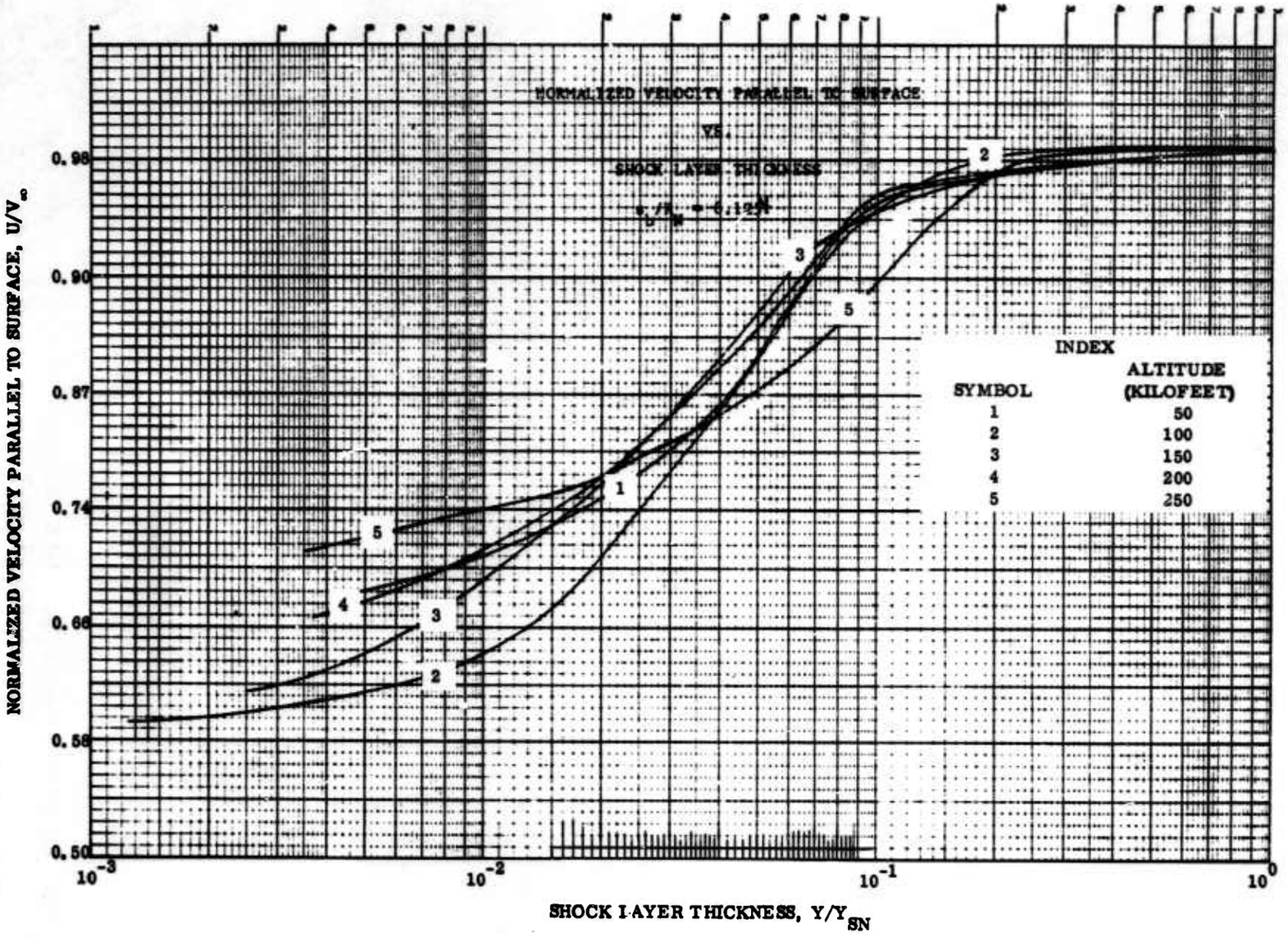

Figure 2.3-21. Normalized Velocity Parallel to Surface vs Shock Layer Thickness; $s_b/R_N = 6.125$

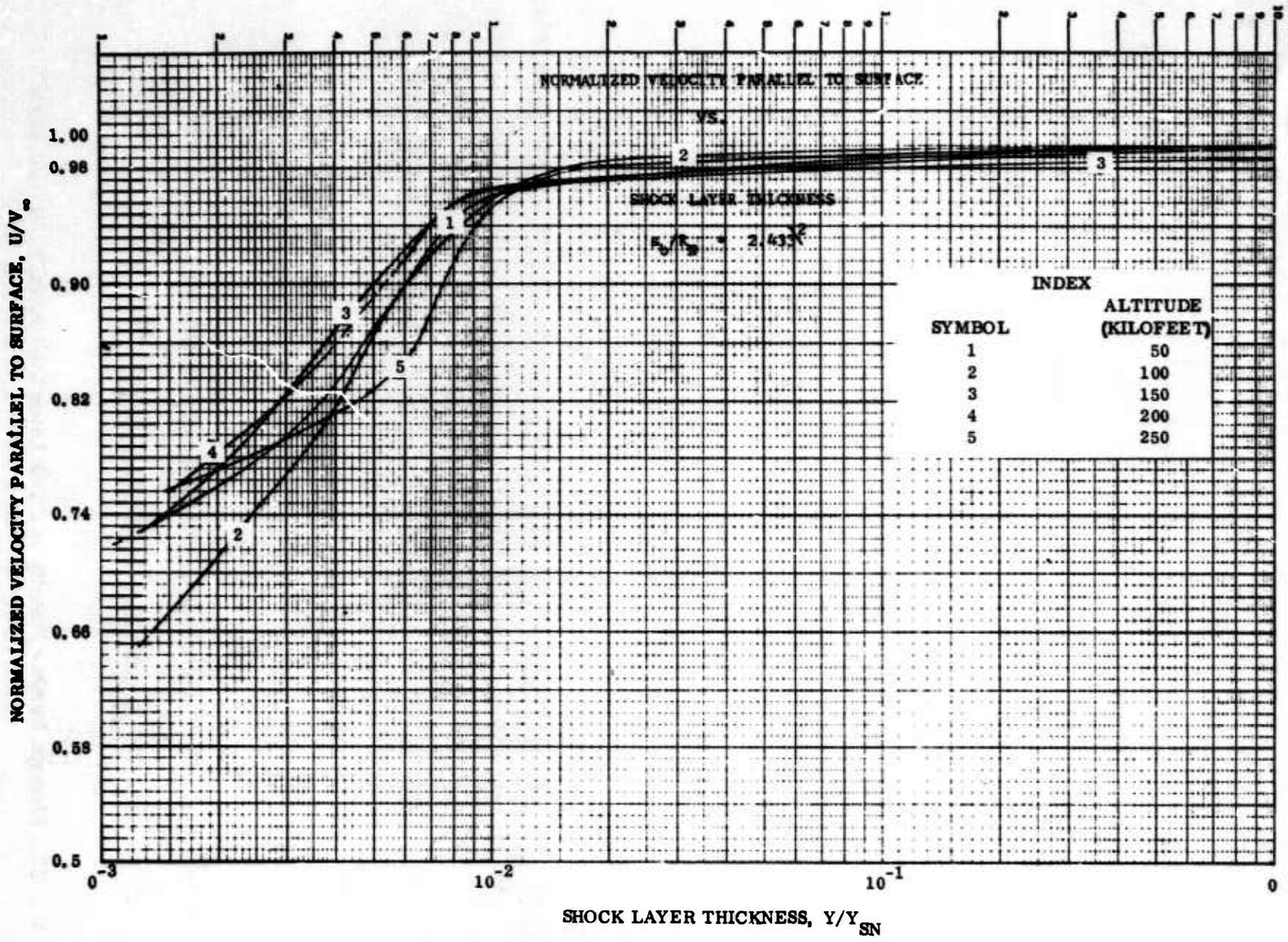

Figure 2.3-22. Normalized Velocity Parallel to Surface vs Shock Layer Thickness; $s_b/R_N = 2.433^2$

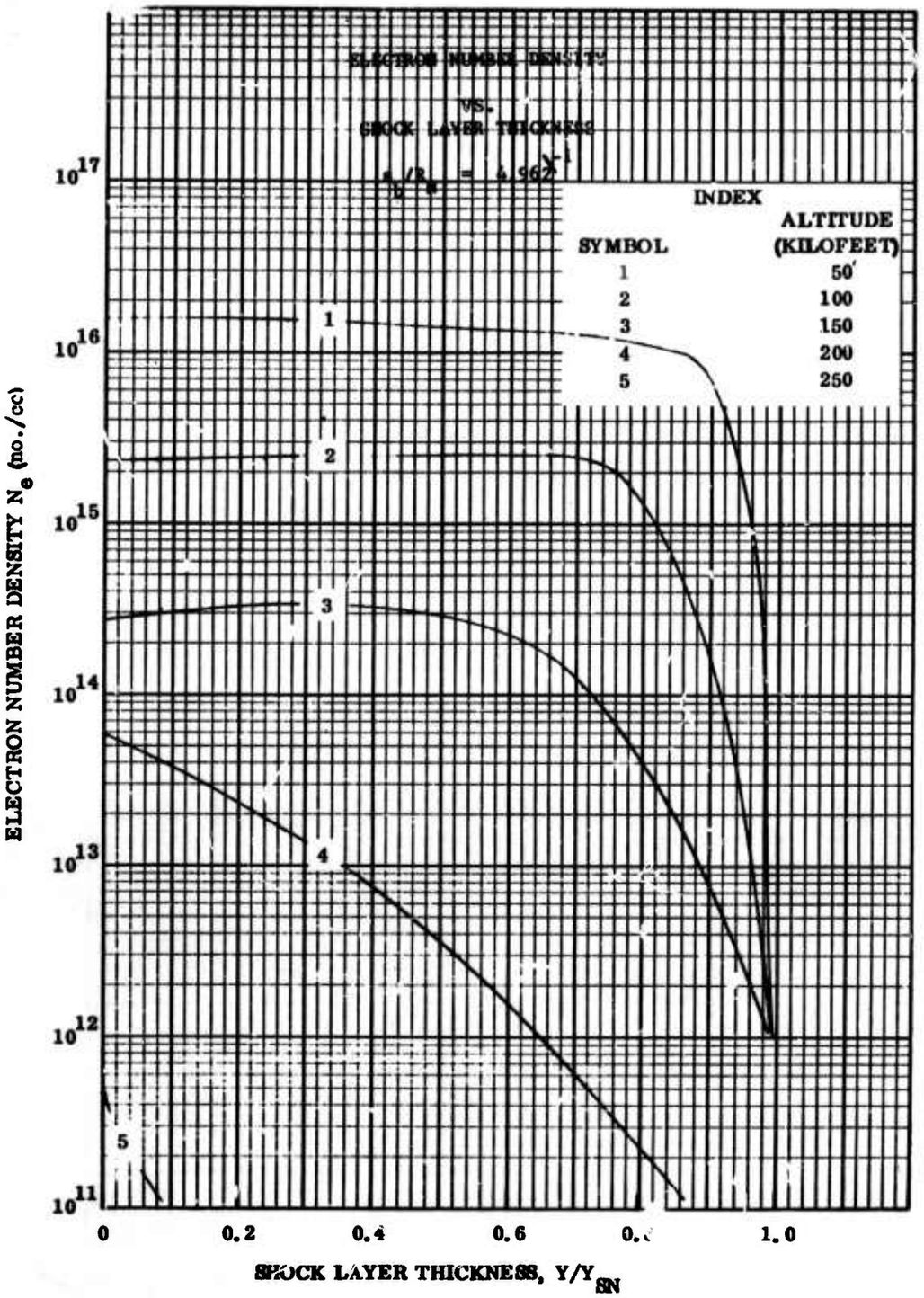

Figure 2. 3-23. Electron Number Density vs Shock Layer Thickness; $\epsilon_b/R_N = 4.962^{\backslash -1}$

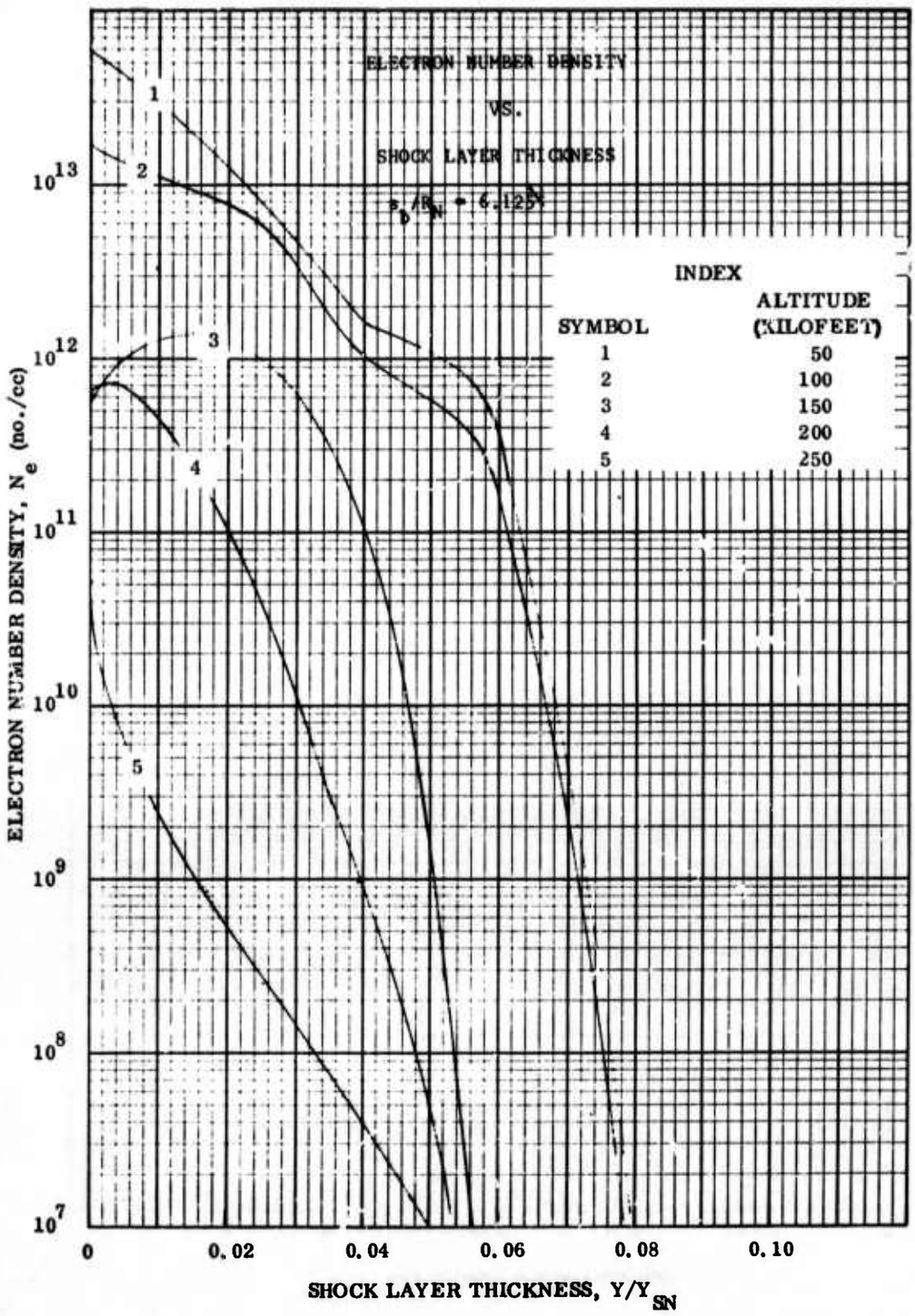

Figure 2.3-24. Electron Number Density vs Shock Layer Thickness; $s_b/R_N = 6.125$ [1]

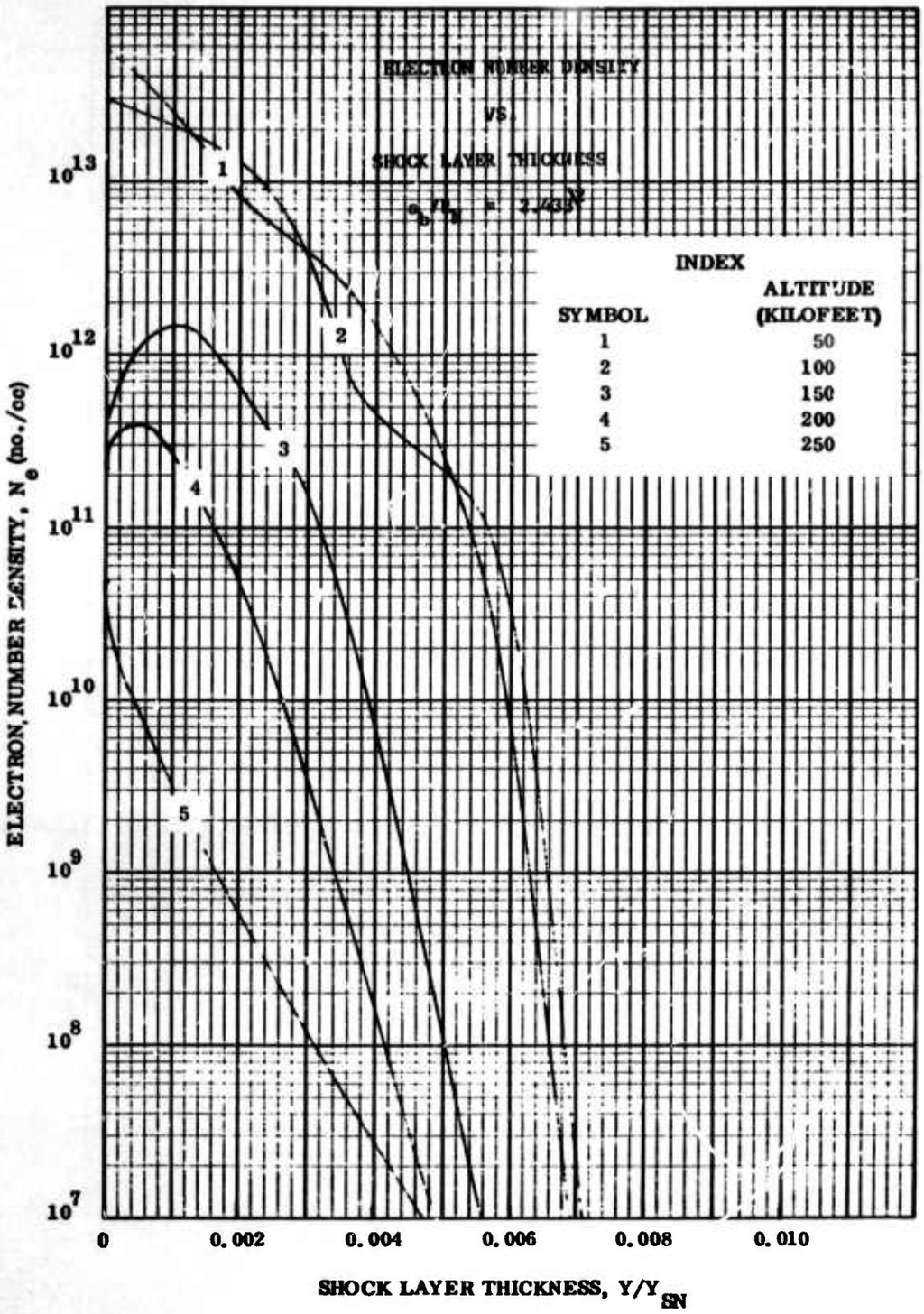

Figure 2.3-25. Electron Number Density vs Shock Layer Thickness; $\varepsilon_b/R_N = 2.433^2$

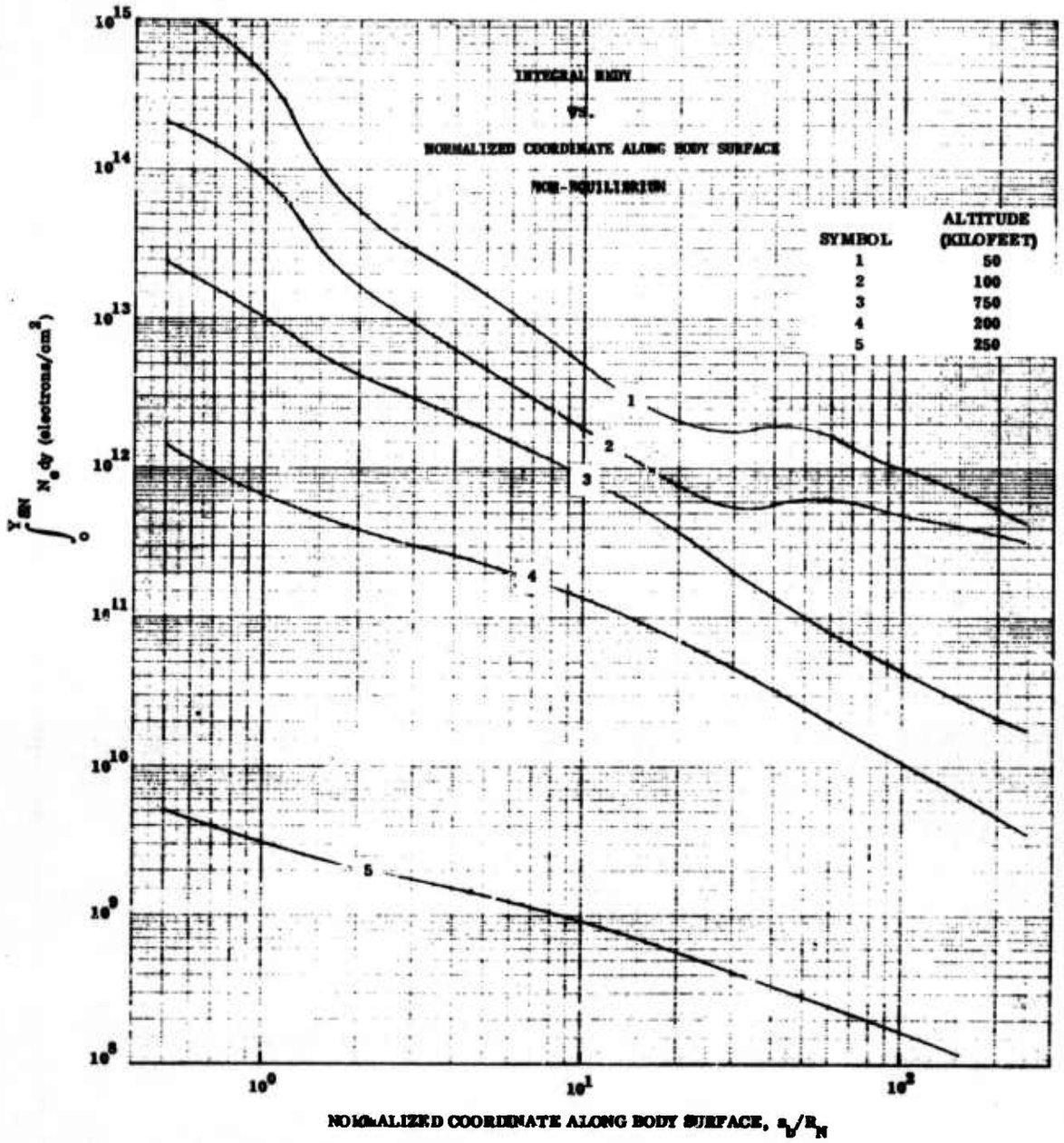

Figure 2.3-26. $\int_0^{Y_{SN}} N_e dy$ vs Normalized Coordinate Along Body Surface; Nonequilibrium

Table 2.3-4. Altitude Dependence of the Species Number Density Normal Profiles, $s_b/R_N = 4.962^{-1}$

Species Number Density (particles per cc)						
Altitude (kilofeet)	Y/Y_{sn}	O_2	N_2	N	O	NO
50	0	5.701^{16}	$2.2.81^{19}$	6.785^{18}	1.296^{19}	1.121^{18}
	2.723^{-1}	6.520	2.378	6.405	1.329	1.203
	7.128	9.689	2.651	5.228	1.418	1.476
	1.000^{0}	6.662^{18}	2.509	0	0	0
100	0	8.290^{14}	2.056^{18}	1.1714^{18}	1.515^{18}	3.810^{16}
	7.742^{-2}	8.742	2.080	1.707	1.526	3.867
	2.429^{-1}	9.556	2.1584	1.660	1.553	4.161
	4.838	1.374^{15}	2.279	1.503	1.566	5.283
	7.005	3.100	2.384	1.195	1.510	8.962
	1.000^{0}	6.399^{17}	2.410	0	0	0
150	0	7.407^{13}	2.097^{17}	2.013^{17}	1.617^{17}	3.753^{15}
	8.064^{-2}	1.126^{14}	2.000	1.838	1.562	4.945
	2.393^{-1}	2.655	2.127	1.484	1.452	8.684
	4.780	7.244	2.187	1.103	1.313	1.693^{16}
	7.044	1.910^{15}	2.238	7.386^{16}	1.113	3.174
	1.000^{0}	6.717^{16}	2.530	0	0	0
200	0	5.316^{13}	3.072^{16}	2.194^{16}	2.080^{16}	1.624^{15}
	7.989^{-2}	1.226^{14}	3.040	1.707	1.828	2.878
	2.706^{-1}	2.772	3.068	1.145	1.541	4.567
	4.782	1.087^{15}	3.220	6.543^{15}	1.324	4.656
	7.098	4.637	3.463	2.973	8.002^{15}	2.588
	1.000^{0}	1.027^{16}	3.867	0	0	0
250	0	1.519^{14}	3.731^{15}	8.299^{14}	1.522^{15}	5.107^{14}
	4.899^{-2}	3.244	3.845	5.944	1.252	4.070
	1.975^{-1}	6.774	4.101	3.517	7.516^{14}	2.238
	4.612	9.954	4.412	1.807	3.348	8.846^{13}
	7.594	1.192^{15}	4.693	6.529^{13}	1.062	2.459
	1.000	1.384	5.211	0	0	0

Table 2.3-5. Altitude Dependence of the Species Number Density Normal Profiles, $s_b/R_N = 6.125$

Species Number Density (particles per cc)						
Altitude (kilofeet)	Y/Y_{sn}	O_2	N_2	N	O	NO
50	0	1.617×10^{16}	1.647×10^{18}	2.962×10^{16}	7.956×10^{17}	7.437×10^{16}
	4.213×10^{-3}	2.259	1.699	2.214	8.009	8.426×10^{17}
	1.247×10^{-2}	5.303×10^{17}	1.844	9.882×10^{15}	7.917	1.144×10^{17}
	2.416	1.366	2.018	3.102	6.872	1.523
	4.088	2.873	2.469	7.620×10^{14}	6.238	1.535
	5.726	5.636	3.169	8.651×10^{13}	3.738×10^{15}	2.473
	7.875	1.094×10^{18}	4.138	1.614×10^{10}	4.946×10^{9}	5.603×10^{15}
	1.145×10^{-1}	1.847	6.955×10^{19}	2.339×10^{-1}	1.399	1.362×10^{9}
	1.000×10^{0}	3.413	1.285×10^{19}	0	0	0
100	0	1.105×10^{12}	1.573×10^{17}	8.295×10^{16}	1.062×10^{17}	7.680×10^{13}
	3.832	1.206	1.636	8.057	1.082	7.306
	8.272	1.351	1.739	7.733	1.128	6.396
	1.279×10^{2}	1.706	1.853	6.865	1.166	6.684
	1.904	2.582	2.048	5.433	1.231	7.097
	2.439	4.354	2.231	3.844	1.286	9.189
	4.013	5.815	2.558	3.992×10^{14}	1.184	8.132×10^{15}
	5.907	4.500×10^{16}	2.898	4.402×10^{13}	4.184×10^{16}	3.001×10^{16}
	8.275	9.934	3.763	2.417×10^{10}	6.729×10^{14}	6.632×10^{14}
	1.166×10^{-1}	1.615×10^{17}	6.082	5.249×10^{2}	1.733×10^{10}	1.936×10^{10}
	2.214	3.493	1.315×10^{18}	1.7518×10^{-15}	1.005×10^{-8}	1.493×10^{-9}
	1.000	3.330	1.254	0	0	0
150	0	2.516×10^{10}	1.998×10^{16}	1.843×10^{16}	1.550×10^{16}	4.343×10^{11}
	7.858×10^{-4}	2.190	1.931	1.624	1.457	4.315
	2.501×10^{-3}	1.809	1.912	1.270	1.352	7.737
	5.777	2.169	1.924	9.210×10^{15}	1.266	2.341×10^{12}
	9.369	5.688	1.945	6.289	1.199	7.363
	1.484×10^{-2}	6.291×10^{11}	1.984	2.900	1.128	3.648×10^{13}
	2.002	2.907×10^{13}	2.008	7.161×10^{14}	1.057	3.083×10^{14}
	3.479	1.645×10^{15}	2.262	4.191×10^{13}	6.532×10^{15}	2.999×10^{15}
	5.117	6.374	2.721	1.633×10^{12}	1.148	7.510×10^{14}
	7.224	1.032×10^{16}	3.890	5.873×10^{8}	1.324×10^{13}	1.199×10^{13}
	1.036×10^{-1}	1.674	6.306×10^{17}	4.821×10^{0}	1.793×10^{8}	2.006×10^{8}
	1.000×10^{0}	3.381	1.273×10^{17}	0	0	0

Table 2.3-5. Altitude Dependence of the Species Number Density Normal Profiles, $s_b/R_N = 6.125 \backslash 1$ (Cont)

Altitude (kilofeet)	Y/Y_{sn}	Species Number Density (particles per cc, O_2	N_2	N	O	NO
200	0	$1.379 \backslash 9$	$2.789 \backslash 15$	$1.780 \backslash 15$	$1.953 \backslash 15$	$2.712 \backslash 11$
	$9.506 \backslash -4$	$2.141 \backslash 10$	2.655	1.205	1.728	$2.111 \backslash 12$
	$3.690 \backslash -3$	$4.829 \backslash 11$	2.659	$6.763 \backslash 14$	1.523	$1.886 \backslash 13$
	$7.235 \backslash -2$	$3.251 \backslash 12$	2.543	3.753	1.393	$6.783 \backslash 14$
	$1.176 \backslash -2$	$1.569 \backslash 13$	2.557	2.199	1.239	$1.982 \backslash 14$
	1.821	8.078	2.674	$7.925 \backslash 13$	1.043	3.214
	2.381	$2.284 \backslash 14$	2.809	2.821	$8.013 \backslash 14$	3.279
	3.932	7.121	3.288	$1.830 \backslash 12$	2.365	$1.164 \backslash 13$
	5.796	$1.126 \backslash 15$	4.305	$2.864 \backslash 10$	$2.317 \backslash 13$	$1.435 \backslash 13$
	7.596	1.568	5.908	$5.450 \backslash 7$	$4.089 \backslash 11$	$3.617 \backslash 11$
	$1.076 \backslash -1$	2.695	$1.015 \backslash 16$	$2.168 \backslash -1$	$3.471 \backslash 6$	$3.877 \backslash 6$
	$1.000 \backslash 0$	5.256	1.980	0	0	0
250	0	$5.390 \backslash 12$	$2.712 \backslash 14$	$5.617 \backslash 13$	$1.223 \backslash 14$	$3.509 \backslash 13$
	$3.088 \backslash -4$	$1.155 \backslash 13$	2.719	3.993	1.068	3.411
	$3.543 \backslash -3$	2.575	2.711	2.228	$7.805 \backslash 13$	2.764
	9.200	4.199	2.769	$1.209 \backslash 12$	5.188	1.959
	$1.668 \backslash -2$	5.486	2.869	$6.996 \backslash 12$	3.460	1.347
	2.511	6.556	3.010	4.101	2.309	$9.121 \backslash 12$
	3.639	7.713	3.234	$2.060 \backslash 11$	1.394	5.583
	4.668	9.840	3.971	$9.455 \backslash 10$	$1.086 \backslash 12$	4.720
	7.038	$1.286 \backslash 14$	4.902	$9.069 \backslash 8$	$2.382 \backslash 11$	1.163
	9.495	1.631	$6.149 \backslash 15$	$2.478 \backslash 3$	$2.902 \backslash 8$	$1.852 \backslash 8$
	$1.411 \backslash -1$	2.745	$1.034 \backslash 15$	$3.099 \backslash -15$	$1.696 \backslash -10$	$1.805 \backslash -11$
	$2.495 \backslash 0$	6.962	2.622	6.678	1.179	2.969
	$1.000 \backslash 0$	7.302	2.750	0	0	0

Table 2.3-6. Altitude Dependence of the Species Number Density Normal Profiles, $s_b/R_N = 2.433^{2}$

Species Number Density (particles per cc)						
Altitude (kilofeet)	Y/Y_{sn}	O_2	N_2	N	O	NO
50	0	1.577^{16}	1.624^{18}	2.858^{16}	7.853^{17}	7.204^{16}
	3.638^{-4}	2.205	1.675	2.132	7.910	8.163
	1.077^{-3}	5.234	1.818	9.445^{15}	7.812	1.115^{17}
	2.092	1.367^{17}	2.030	3.154	6.929	1.532
	3.575	3.003	2.327	8.382^{14}	4.986	1.864
	5.073	6.048	2.962	7.207^{13}	2.577	1.583
	7.011	1.103^{18}	4.162	1.668^{10}	4.990^{15}	5.729^{15}
	1.013^{-2}	1.847	6.955	2.341^{-1}	1.400^{9}	1.363^{9}
	1.000^{0}	3.467	1.306^{19}	0	0	0
100	0	7.503^{12}	1.362^{17}	5.191^{16}	8.570^{16}	4.821^{14}
	1.181^{-4}	7.409	1.373	5.150	8.621	4.758
	3.755	7.253	1.415	4.980	8.801	4.600
	8.123	6.793	1.497	4.681	9.160	4.224
	1.253^{-3}	6.877	1.609	4.173	9.618^{17}	3.984
	1.852	7.504	1.806	3.293	1.044^{17}	3.626
	2.349	1.049^{13}	2.009	2.313	1.126	3.696
	3.710	6.429^{15}	2.499	3.797^{13}	1.137	8.444^{15}
	5.265	4.653^{16}	2.866	3.930^{10}	4.199^{16}	2.334^{16}
	7.216	1.005^{17}	3.808	2.694^{2}	7.180^{14}	7.368^{14}
	1.001^{-2}	1.625	6.120	5.739^{-20}	1.765^{10}	1.968^{10}
	1.871	3.449	1.299^{18}	4.914^{-8}	7.574^{-8}	1.109^{-8}
	1.000^{0}	3.357	1.264	0	0	0
150	0	2.125^{10}	1.927^{16}	1.728^{16}	1.482^{16}	4.386^{11}
	6.892^{-5}	1.960	1.929	1.589	1.444	5.525
	2.177^{-4}	1.914	1.934	1.264	1.363	1.031^{12}
	4.986	2.544	1.960	9.300^{15}	1.288	3.102
	8.056	7.945	1.989	6.397	1.226	9.555
	1.272^{-3}	1.030^{12}	2.034	2.978	1.155	4.937^{13}
	1.713	3.146^{13}	2.064	7.684^{14}	1.086	3.290^{14}
	2.973	1.866^{15}	2.351	4.604^{13}	6.937^{15}	2.487^{15}
	4.366	6.355	2.814	2.271^{12}	1.379	1.166
	6.160	1.063^{16}	4.009	8.016^{8}	1.499^{13}	1.399^{13}
	8.868	1.749	6.587	8.923^{0}	1.369^{8}	2.189^{8}
	1.000^{0}	3.405	1.282^{17}	0	0	0

Table 2.3-6. Altitude Dependence of the Species Number Density Normal Profiles, $s_b/R_N = 2.433^{2}$ (Cont)

Species Number Density (particles per cc)						
Altitude (kilofeet)	Y/Y_{sn}	O_2	N_2	N	O	NO
200	0	9.286^{8}	2.793^{15}	1.782^{15}	1.956^{15}	2.599^{11}
	7.827^{-5}	9.822^{9}	2.659	1.206	1.731	1.525^{12}
	3.059^{-4}	1.740^{11}	2.562	6.651^{14}	1.529	9.520
	6.022	1.600^{12}	2.544	3.375	1.411	3.545^{13}
	9.835	1.277^{13}	2.590	1.370	1.304	1.117^{14}
	1.524^{-3}	7.330	2.726	4.590^{13}	1.110	2.763
	1.987	1.864^{14}	2.868	2.094	8.794^{14}	3.758
	3.255	6.715	3.355	2.185^{12}	2.977	1.929
	4.795	1.126^{15}	4.330	3.440^{10}	2.802^{13}	1.971^{13}
	6.298	1.593	3.002	2.960^{7}	4.602^{11}	4.180^{11}
	8.955	2.702	1.017^{16}	1.305^{-1}	3.619^{6}	4.020^{6}
	1.000^{0}	5.259	1.981	0	0	0
250	0	1.914^{12}	3.062^{14}	3.896^{13}	1.516^{14}	2.379^{13}
	7.526^{-5}	4.776	3.023	2.435	1.338	3.218
	3.225^{-4}	1.518^{13}	3.014	1.070	1.037	3.920
	8.234	3.244	3.092	4.622^{12}	7.464^{13}	3.525
	1.480^{-3}	4.892	3.220	2.261	5.362	2.738
	2.217	6.404	3.389	1.137	3.767	1.979
	3.206	8.080	3.649	4.733^{11}	2.319	1.236
	4.115	9.277	3.881	2.202	1.476	7.957^{12}
	6.308	1.241^{14}	4.758^{15}	1.595^{10}	3.015^{12}	1.741
	9.209	2.670	1.005^{15}	1.328^{3}	1.716^{8}	1.831^{8}
	1.909^{-2}	6.824	2.570	5.798^{-15}	7.851^{-10}	1.857^{-10}
	1.000^{0}	7.469	2.813	0	0	0

the body surface with altitude as a parameter. Some of the more noteworthy aspects of these results are discussed in the following paragraphs.

It is worth noting in Figures 2.3-11, 2.3-12 and 2.3-13 that the pressure profiles obtained from the perfect gas or equilibrium flow fields actually follow the free stream Mach number variation rather than the altitude variation. Also, for these pressure profiles, which are derived from the perfect gas or equilibrium streamwise pressure distributions and reproduced during the construction of the approximate nonequilibrium flow field, the pressure behind the shock is replaced by the value from the thermal equilibrium frozen shock flow solution. This change at $Y/Y_{SN} = 1$ is particularly noticeable on the first normal, where the result is a lower value for the equilibrium cases and a higher value for the perfect gas case.

Some attention should also be directed to the development of an off-wall peak in the temperature profiles back on the conical surface (Figures 2.3-15 and 2.3-16) as the altitude is increased. This trend is unquestionably one of the more marked effects of nonequilibrium flow, inasmuch as the temperature for equilibrium flow decreases monotonically from the wall to the shock (except in the region where the streamlines have traversed that portion of the shock where the minimum shock angle occurs as a result of the overexpansion).

2.4 FUTURE FLOW FIELD WORK

As required for use in the antenna breakdown study, inviscid flow properties at several altitudes above 175 kilofeet will be obtained for the limiting cases of no vibrational excitation and full vibrational excitation, for critical comparison.

Chemically reacting boundary layer calculations for ablation product contaminated flow, including the important metallic trace impurities, will be made at various altitudes to determine viscous and contamination effects on plasma properties.

Furthermore, a survey of the current state of the art in body flow field analysis will be made and reported late in the contract period.

SECTION 3

ANTENNAS AND PROPAGATION

3.1 ANTENNAS

3.1.1 ECM ANTENNAS

This subject is covered in entirety in Volume II of this report.

3.1.2 ANTENNA FIELD THEORY

The purpose of this discussion is to survey the methods of calculating antenna near-field distributions, which should be known before antenna breakdown and reentry-induced plasma effects can be analyzed.

In general, the complete radiated fields of a given antenna must be calculated in terms of the antenna geometry, current distribution, and wavelength. For prediction of the effects of reentry plasmas on the antenna properties and patterns, it will be necessary to consider the antenna as a finite, continuous source. Thus calculation of the transmitted power, patterns, and polarization becomes a solution of an exact boundary-value problem. However, since the wave equation

$$\nabla \times \nabla \times \vec{E} = \vec{p}\,\delta\,(\vec{r} - \vec{a})$$

is separable in only a few restricted coordinate systems (e.g., spheroidal and infinite cylindrical), approximate methods usually must be employed.

A common method is an integral equation approach. From Huygen's principle we can evaluate the fields external to a surface by the specification of the charges and currents on that surface. In terms of the magnetic vector potential $\vec{A}$,

$$\vec{H} = \frac{1}{\mu_o} \nabla \times \vec{A}, \qquad (3.1.2\text{-}1)$$

$$\vec{E} = -\frac{j}{\omega\mu\epsilon} \nabla \times \nabla \times \vec{A} \qquad (3.1.2\text{-}2)$$

For a line source of length L,

$$\vec{A} = \vec{k} A_z = \frac{\vec{k}\mu_o}{4\pi} \int_{-L/2}^{L/2} I(z') \frac{e^{-j\,kr'}}{r'} dz \qquad (3.1.2\text{-}3)$$

where the integration is over the source coordinates (x', y', z') and we have assumed the source current I(z') along the z' axis. Now, in principle, the Poynting vector, $\vec{S} = \vec{E} \times \vec{H}$, is the solution of our problem, specified by Equations 3.1.2-1 through 3.1.2-3. However, the integral (Equation 3.1.2-3) must be evaluated approximately. It is convenient to consider the fields in three different regions;

$r < 0.62\sqrt{\frac{L^2}{\lambda}}$, near field,

$0.62\sqrt{\frac{L^2}{\lambda}} \leq r \leq \frac{2L^2}{\lambda}$, Fresnel zone,

$r > \frac{2L^2}{\lambda}$, far or radiation zone.

If the source were a surface or a volume, then the integral in (Equation 3.1.2-3) would be modified accordingly. The essential problem is the determination of the current distribution, I (z'). The general theory in terms of arbitrary source current distributions has been given by Silver[9]. We will be mainly interested in the solutions for dipoles (finite cylindrical antennas) and for traveling-wave antennas (helices). The procedures required in the analysis of these two types can then be applied to other types of antennas.

Traveling-wave antennas may be represented by letting the current in Equation 3.1.2-3 become sinusoidal, so that

$$I(z') = \sum_{n=-\infty}^{\infty} I_n \exp\left[-j\left(n\pi z'/L\right)\right] \qquad (3.1.2\text{-}4)$$

$$I_n = \frac{1}{2L} = \int_{z}^{z+L} I(z') \exp\left[j\left(n\pi z'/L\right)\right] dz' \qquad (3.1.2\text{-}5)$$

Thus the source is represented as a sum of traveling waves. The near fields of a line source[10] represented in this manner can be evaluated by quantizing the length into segments so short that the field point is in the far field of the segment while still in the near field of the whole antenna. Thus the integral of Equation 3.1.2-3 is broken up into N integrals, in each of which the current I is a constant. The integration is simplified so that the near-field is of the form

$$E_z = \frac{-j\omega\mu L}{4N\pi} \sum_{n=1}^{N} I_n \frac{\exp(-j k r_n)}{r_n} \sin^2\theta \frac{\sin \chi_n}{\chi_n}$$

where

$$\chi_n = \left[\frac{k(z - z_n)}{r_n} - \beta_n\right]\frac{L}{2N}$$

The same method may be generalized to rectangular and circular sources.

An important type of traveling-wave antenna is the helix, which is a slow-wave structure. Using the sheath helix approximation, this problem can be solved exactly[11,12].

A complete discussion of the properties of single-wire and multiwire helices is given by Watkins[13] with impedance calculations, k - β diagrams, and field patterns. In addition, Walter[10] discusses helices in the context of traveling-wave structures. The effects of ionized atmospheres on the transmission line characteristics of helices has been discussed by Neurather, et al.[14]

The dipole or cylindrical antenna has been analyzed thoroughly by King[15]. In order to calculate the radiation patterns, impedances, and near fields of finite cylindrical antennas, it is necessary to solve the well-known Hallen integral equation[16]. This was done using an iterative method assuming a sinusoidal current distribution, as outlined in Kraus[17]. We then obtain well-used formulas for the impedances and near-fields as a function of wavelength and antenna dimensions. A more accurate determination has been made by King and Middleton[18] assuming a $(\sin\theta)/\theta$ initial current distribution. Over the years, a voluminous literature has been generated on the subject[19,20,21]. The essential problem is determining the axial current distribution; the calculation of the fields and impedance follows directly from the methods given in References 15 and 17. Since the initial current distribution is so important, there can be no true separation from plasma effects. The analysis of dipoles in ionized atmospheres has been performed by Balmain[22], who assumes a triangular current distribution, and by Cook and Edgar[23], who solve for the current distribution assuming that the electron velocity vanishes at the edge of the plasma. For the frequency and power ranges under consideration, dipole (or multipole) radiators are more important; however, calculations for loops similar in method have been given by Iizuka and King[24].

3.2 LINEAR PLASMA EFFECTS

As indicated in Section 3.1.2 on antenna field theory, the near fields and radiated fields of a radiating source are determined by the current and charge distributions of the source. The presence of a plasma layer will affect the current distribution and impedance of an antenna since, basically, the plasma dielectric constant differs from that of free space,

$$\frac{\epsilon_p}{\epsilon_o} = 1 - \frac{\omega_p}{\omega\,(\omega + j\nu_c)}, \qquad (3.2\text{-}1)$$

$$\omega_p^2 = \frac{ne^2}{m\epsilon_o} , \qquad (3.2\text{-}2)$$

where

ν_c = Electron collision frequency

n = Electron density

e = Electron charge

m = Electron mass

Thus the wave number

$$k = \frac{2\pi}{\lambda} = \frac{\omega}{c} = \frac{2\pi\nu}{c} , \; c = \frac{1}{\sqrt{\mu_o \epsilon_o}} \qquad (3.2\text{-}3)$$

and propagation constant, γ, must be calculated in order to determine the field configurations. However, the presence of the plasma layer allows the existence of many modes of propagation in addition to the continuous spectrum of free-space wavelengths. Therefore, the analysis is made convenient by first considering the possible modes in a simple structure, e.g., a plasma layer over a plane surface, and then considering other, more practical geometries.

The total field of this antenna configuration can be related to the impedance and dimensions of the source antenna and the plasma layer by integral transform techniques. Applying the Huygens theory of Equation 3.1.2-1, 3.1.2-2 and 3.1.2-3., we are led to the evaluation of the integral,

$$E_y(x,z) = \frac{-j\omega\mu_o}{4\pi} \int_C \left\{ \frac{\exp[-j K_o (x-\delta)]}{K_o} + \Gamma \frac{\exp[-j K_o (x+\delta)]}{K_o} \right\} \exp(-\gamma z)\, dz \qquad (3.2\text{-}4)$$

where the propagation constants in the z-direction,

$$K_1 = (k^2 \epsilon + \gamma^2)^{1/2}, \qquad (3.2\text{-}5)$$

$$K_o = (k^2 + \gamma^2)^{1/2}, \qquad (3.2\text{-}6)$$

and the impedance of the plasma layer is

$$\Gamma = \frac{K_o + j K_1 \cot K_1 d}{K_o - j K_1 \cot K_1 d} \qquad (3.2\text{-}7)$$

Thus, evaluation of the field E_y depends on the location of the singularities in the integrand of Equation 3.2-4. If we make the transformation

$$\gamma = \alpha + j\beta^2 \rightarrow j k \nu = j k (\xi + j \eta) \qquad (3.2\text{-}8)$$

the steepest descent contour C of Equation 3.2-4 is shown in Figure 3.2-1. The location of the poles, given by Equations 3.2-5, 3.2-6, and 3.2-7, relate the plasma properties to the antenna fields. The formulation may again be generalized to two- and three-dimensions.

The effect of a plasma sheath on an antenna has been studied by many authors. Wait[25] has analyzed the effect of a thin plasma sheet on a dipole antenna. He uses a direct solution of the boundary-value problem in order to calculate the radiation patterns. He considers electron collisions and obtains results with and without an impressed magnetic field. He has

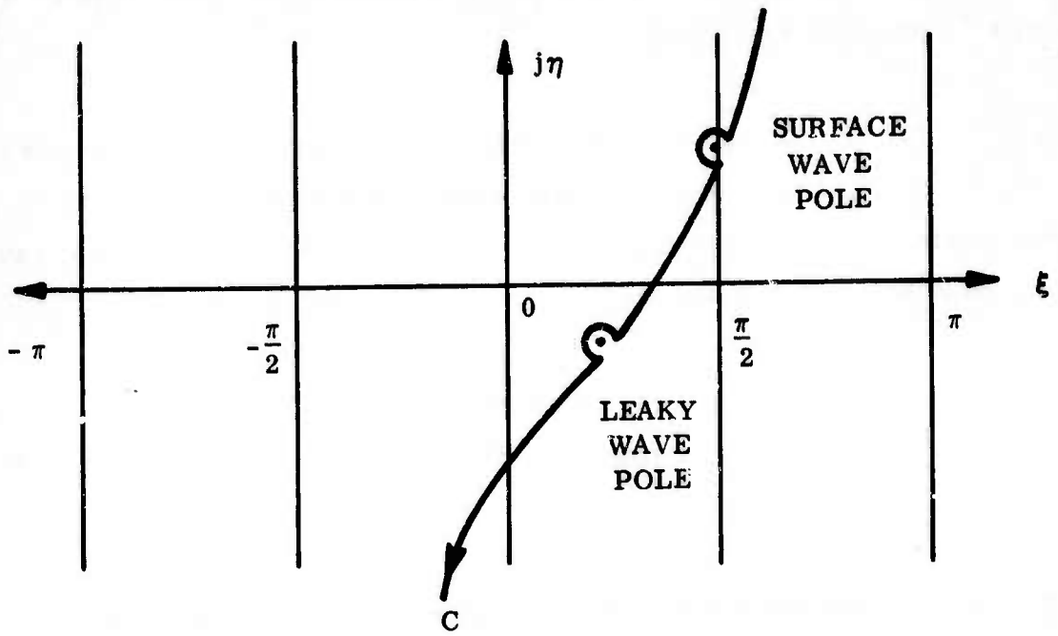

Figure 3.2-1. Steepest Descent Contour C

formulated the problem in terms of the radial Hertz potential and thus has obtained a splitting of the field into a radiation field (saddle-point contribution) and surface field (pole contribution). The same configuration has been treated in great detail by Tamir and Oliner[26], Wenger[27], Bernard and Ishimaru[28], and Walter[10].

The propagation constants, K, and impedances, Γ, may be calculated by variational methods[26]. Thus the change in propagation constant, β, with variation in plasma dielectric constant, ϵ, is

$$\beta - \beta_o \doteq \omega \frac{\int_S [\Delta\epsilon \vec{E} \cdot \vec{E}_o^* + \Delta\mu_* \vec{H} \cdot \vec{H}_o] \, d\vec{S}}{\int_S (\vec{E}_o^* \times \vec{H} + \vec{E} \times \vec{H}_o^*) \cdot d\vec{S}}$$

The variational method can also be used to determine the effects of slots on the propagation constant of a waveguide or radiating structure, which is useful in determining the near-field patterns for the previous section.

References 28 and 10 present the effects on the radiation patterns of the various pole contributions. The classification into pole contributions (leaky-wave, backward and forward waves, surface waves, etc.) is useful in studying the myriad of possible propagation modes discussed in References 26 and 27.

The calculation of the dipole fields in the presence of a plasma layer has been done very completely by Baños.[30] He gives complete formulas and radiation patterns for the case of an infinitesimal (Hertz) dipole.

An alternate representation is obtained by angular transformation techniques rather than normal mode formulations based upon orthogonal coordinates. Thus the residue series obtained by a Watson transformation[31,32] can be evaluated. This has been discussed by Wait[33] and by Bremmer.[34]

The linear effects of plasma sheaths have been calculated for the spherical case by Wait and Spies[35] and for the spheroidal case by Yeh.[36] These two particular geometries can be solved by exact boundary-value methods and thus provide convenient, although approximate, calculations of linear plasma effects. The slotted cylindrical antenna, which is a useful approximation to the reentry vehicle, has been studied in great detail by many authors, particularly Smith and Golden,[37] Swift,[38] and Rusch.[39] The cylindrical geometry is important when the wavelength is comparable to the vehicle size, for then the curvature of the vehicle and the surrounding antenna must be considered. Since the wave equation is separable in cylindrical coordinates, this is a suitable mathematical model which simulates the aft portion of many reentry vehicles. The finite slot should be the appropriate representation of the source, but this involves complicated mathematical procedures which restrict complete pattern calculations to plasma sheaths that are homogeneous and loss-less[39,40,41]. The problem of the homogeneous, lossy plasma has been solved by Sengupta[42] who included

collisions through the use of a thin sheath and high and low frequency approximations. However, the practical solutions of these equations, in general, are not specifiable because the plasma properties may vary arbitrarily within the shock layer. Therefore, analytical techniques or WKB approximations are not realistic for many problems of interest and must be abandoned in favor of exact numerical techniques. The inhomogeneous case is solved by Tyras and Harley,[43] who consider the plasma as a multilayered series of lossy, homogeneous plasma slabs.

This approach requires application of the boundary conditions a great many times and may lead to computational difficulties. An alternate scheme is to integrate the wave equation directly.[44,45] Swift[38] explains this method in detail and gives antenna patterns for homogeneous sheaths of arbitrary thicknesses and with ν_c/ω varying from 0 to 0.30.

The effects of a conical plasma sheath are important for nose antennas where the boundary layer is ionized. Since the wave equation is not separable in these coordinates, various mathematical devices have been applied. Yeh[46] uses an application of Sommerfield's complex order wave functions to obtain the far-field radiation patterns. His analysis is especially applicable to high frequency ($ka > 3$) cases. In addition, his formulation of the problem allows consideration of an infinite sheath whose thickness and electron density vary linearly with radial distance. Baños et al[47] have given a complete analysis of the radiation pattern distortion by an infinite conical plasma sheath around an electric dipole. Using the Watson transformation, they obtain a residue series representation of the radiated fields. This analysis is useful since it separates the fields into surface-wave and dipole contributions. The plasma model used was collisionless and homogeneous. Jordan et al[48] have extended the analysis to include electron collisions. Pridmore Brown[49] has used the Wiener Hopf technique to extend the Baños solution to the finite length cone. Again these analyses hold for homogeneous thin plasmas.

Finally, we may note the utility of the linear plasma solutions in obtaining nonlinear calculations. Menzel[50] gives a general discussion of the construction of solutions to problems including nonlinear interactions of electromagnetic waves with an ionized atmosphere. The generation of

electro-acoustic modes[51] may also be considered as a phenomenon contributing to power absorption of a transmitting antenna in a reentry environment.

3.3 ANTENNA BREAKDOWN

This section discusses theoretical methods of predicting the electric field intensity at which microwave breakdown of the atmosphere takes place. Breakdown electric field is a useful parameter because it can be related to a minimum number of independent variables. On the other hand, the power handling capability of an antenna depends on the field distribution of the particular antenna.

The discussion covers static breakdown and reentry effects. Static breakdown is defined as dielectric breakdown in an undisturbed environment. The subject of reentry effects is concerned with breakdown of an antenna mounted on a vehicle in hypersonic flight in the atmosphere.

3.3.1 STATIC BREAKDOWN

The subject of microwave breakdown in gases has been thoroughly surveyed by MacDonald in a recent book.[52] This book presents practically all of the basic theory of high frequency gas discharges. Moreover, it indicates how breakdown field strengths can be calculated reliably. The book is thus useful in providing the basic physical theories on the subject as well as the practical tools needed for applications. In addition, a whole chapter is devoted to experimental methods.

Let us now give a brief summary of basic breakdown theory, beginning with a qualitative description of the breakdown process. The impressed electromagnetic field exerts force on any free electrons which may be present in the gas. Through the process of collisions of electrons with neutral gas particles, the field does work on the electrons, raising their average temperature well above that of the gas. Ionization of neutral particules by impact of high energy electrons competes with electron attachment to neutral particles to give a net rate of electron population gain. This net ionization rate competes with losses by diffusion until the point is reached where the ionization builds up at a very rapid rate and the gas

becomes conducting. The various collision processes are very important in determining breakdown, in that they control the energy distribution as well as the number density of electrons.

The kinetic theory approach to breakdown prediction treats the electron distribution function F (v, r, t), which represents the number of electrons with velocities close to v, in a small volume of space at the point r, and at the time t. This distribution function obeys the Boltzmann equation[53, 54]

$$\frac{\partial F}{\partial t} + \vec{v} \cdot \nabla F + \vec{a} \cdot \nabla_v F = C \qquad (3.3.1\text{-}1)$$

where ∇ is the gradient in configuration space, ∇_v is the gradient in velocity space, a is the acceleration, and C represents the effects of collisions.

The collision term C may be written as an integral involving the distribution function and the collision cross section,[54] and hence knowledge of collision cross section as a function of electron velocity is sufficient in principle to solve the Boltzmann equation. However, the difficulties involved are so great that accurate results are possible in only a few cases.

Hydrogen and helium have practically constant collision frequencies above an energy of about 3 or 4 electron volts, and this fact has been used by MacDonald and Brown[55, 56] and Reder and Brown[57] to calculate breakdown fields for these two gases and for admixtures of mercury. The results agree very well with experiment, especially for the case of helium containing a small amount of mercury. The presence of mercury serves to convert the metastable excitation level of helium to ionization of mercury by an exchange reaction. This has the effect that the gas has no excitation levels below the effective ionization level, greatly simplifying the analysis. The theoretical results for neon and neon-argon mixtures, for which the collision frequency is approximately proportional to the square root of the electron energy, do not agree with experiment quite so well as for constant collision frequency gases.

Most practical microwave breakdown theory is based on phenomenological models, because of the difficulties encountered with collisional processes in the kinetic theory approach. In the phenomenological theory, the electron continuity equation is written in terms of macroscopic rate constants, which can be determined experimentally as functions of electric field and pressure. The electron continuity equation is written as

$$\frac{\partial n}{\partial t} - \nabla \cdot \vec{\Gamma} - P = 0 \qquad (3.3.1\text{-}2)$$

where n is the electron density, $\vec{\Gamma}$ is the electron flux, and P is the net effect of all sources and sinks.

Free diffusion of electrons applies to static breakdown, where the initial electron density is very low. Then

$$\vec{\Gamma} = - \nabla(Dn) \qquad (3.3.1\text{-}3)$$

where D is the diffusion coefficient. When the net ionization rate per electron is represented by the symbol ν, the continuity equation may be written as

$$\frac{\partial n}{\partial t} = \nabla^2 (Dn) + n\nu \qquad (3.3.1\text{-}4)$$

This equation is generally solved by assuming separability, using

$$\nabla^2 (Dn) = - \frac{Dn}{\Lambda^2} \qquad (3.3.1\text{-}5)$$

where Λ is the diffusion length. Thus

$$\frac{dn}{dt} = \left(\nu - \frac{D}{\Lambda^2} \right) (n) \qquad (3.3.1\text{-}6)$$

The Townsend criterion, carried over from the theory of direct current discharges, has been shown by Herlin and Brown[58] to apply to microwave discharges. According to this criterion, the breakdown point is reached when the right hand side of Equation 3.3.1-6 is zero, since a slightly higher electric field would cause the runaway production of electrons.

When either the electric field or the electron mobility is not uniform in space, as would be the case in antenna breakdown, the diffusion equation must be solved in the form of Equation 3.3.1-4, with the left hand side set equal to zero. However, it is possible to use an effective diffusion length which can be derived from the solution of the diffusion equation. For example, Herlin and Brown[59] derived the solution for a TM_{010}-mode cylindrical cavity and MacDonald and Brown[60] derived the results for a spherical cavity.

It can be shown,[52] through certain considerations in the kinetic theory, that the important parameter with respect to electric field E and the microwave radian frequency ω is

$$E_e^2 = \frac{\nu_c^2 E^2}{\nu_c^2 + \omega^2} \qquad (3.3.1\text{-}7)$$

where E_e is the effective field and ν_c is the collision frequency. The effective field concept is useful in the phenomenological theory of breakdown, as in the analysis of Brown,[61] Rose and Brown,[62] and Gould and Roberts.[63] The Townsend criterion is written as

$$\nu_i = \nu_a + \frac{D}{\Lambda^2} \qquad (3.3.1\text{-}8)$$

where ν_i and ν_a are the ionization and attachment frequencies, respectively. The first Townsend coefficient α is used in place of ν_i according to the equation

$$\nu_i = \alpha \mu E_e \qquad (3.3.1\text{-}9)$$

where μ is the dc mobility. The ratio of diffusion coefficient to mobility is invoked to give the relation

$$\frac{\alpha}{p} = \frac{\beta}{p} + \frac{2}{3} \frac{u}{(p\Lambda)(E_e\Lambda)} \qquad (3.3.1\text{-}10)$$

where p is pressure, u is average electron energy, and β is the number of attachments per centimeter of path length. Data exists for α/p, β/p, and u as functions of E/p in air.[61,64] Hence, Equation 3.3.1-10 may be used to give Ee/p as a function of $p\Lambda$, provided E_e can be calculated.

The difficulty connected with the phenomenological theory is that the effective field is not a sound concept, since the collision frequency is not constant. Brown[61] obviates this difficulty by calculating an effective constant collision frequency from the measured ac mobility, using

$$\mu_{ac} = \frac{(e/m)\,\nu_c}{\nu_c^2 + \omega^2} \qquad (3.3.1\text{-}11)$$

where e/m is the ratio of charge to mass for the electron. He gets a value of ν_c equal to $4.3 \times 10^9 p$. The results of breakdown calculations then agree with experimental data fairly well over a limited range of pressures.

It appears that the most reliable and generally useful method of calculating breakdown is that given by MacDonald.[52] This method is a phenomenological one which uses the effective field concept in a way which is much less sensitive to the specific form of collision frequency assumed than is the above method. The diffusion coefficient can be calculated from the variation of collision frequency with electron energy, if the electron energy distribution is assumed; however, it can be shown that the form of the distribution function has little effect on the result. Hence the approximation of MacDonald, Gaskell, and Gitterman[65] works well.

$$Dp = \left(29 + \frac{0.9\,E_e}{p}\right) 10^4 \text{ cm}^2 - \text{Torr/sec} \qquad (3.3.1\text{-}12)$$

This equation was derived from assuming a linear dependence of Dp on average electron energy in terms of the latter's experimentally determined dependence on E/p. Equation 3.3.1-12 is equivalent to

$$\frac{D\lambda}{\Lambda^2} = 10^4 \left(\frac{\lambda}{\Lambda}\right)^2 S \qquad (3.3.1\text{-}13)$$

where λ is the wavelength and

$$S = \frac{1}{p\lambda}\left[29 + \frac{0.9\,E\lambda}{\left[(p\lambda)^2 + (35.6)^2\right]^{1/2}}\right] \qquad (3.3.1\text{-}14)$$

where $E\lambda$ is in volts and $p\lambda$ is in Torr-cm.

The net ionization rate ν may be related to the electric field and the pressure by using experimental breakdown data. The result is shown in Figure 8-18 of Reference 52 in terms of $\nu\lambda$ versus $p\lambda$ for fixed values of $E\lambda$. Figure 8-19 in Reference 52 shows a plot of Equation 3.3.1-14. The solution to a given problem in continuous wave breakdown in air is found by the points of intersection of these two sets of curves, as shown in Figure 8-20 in Reference 52, since at breakdown, $\nu\lambda$ is equal to $D\lambda/\Lambda^2$. The curves are superimposed such that the point S = 1 coincides with the point $\nu\lambda = 10^4 (\lambda/\Lambda)^2$. Thus, when the wavelength and the diffusion length are known, the breakdown field versus pressure can be determined quite easily by this method.

The above method of calculating continuous wave breakdown can be generalized to include pulse (or finite time) effects, following the approach of Gould and Roberts.[63] For example, for pulsed breakdown at low pulse repetition rate, the net ionization frequency is determined by

$$\nu_b \tau = \ln (n_b/n_o) \qquad (3.3.1\text{-}15)$$

where τ is the pulse length, n_b is the electron density required for breakdown, and n_o is the initial electron density. The value of n_b is usually taken as the critical value, $10^{13}/\lambda^2$, where λ is in cm and n_b is in cm^{-3}; and n_o is a fairly small number. For a given pulse length, Equation 3.3.1-15 determines ν_b, which is actually related to ν of the CW analysis by

$$\nu_b = \nu - \frac{D}{\Lambda^2} \qquad (3.3.1\text{-}16)$$

The procedure is to estimate E from continuous wave theory and to determine D from Equation 3.3.1-13. Then ν is determined from Equation 3.3.1-16. This gives E from CW theory, and the process can be iterated to determine E more accurately. In case of rapid pulse repetition rates, the decay time of the afterglow between pulses must be taken into account. Then the breakdown criterion is that the buildup of ionization during the pulse is just equal to the decay between pulses. A slightly greater net ionization rate during the pulse would give a runaway condition. As the pulse repetition rate is increased, the breakdown field approaches the continuous wave case.

3.3.2 REENTRY EFFECTS

The effects of reentry on the breakdown conditions are to change the rates at which the various breakdown controlling processes proceed and to add processes not considered in the static breakdown case. The following paragraphs will discuss some of the changes mentioned in the literature and will give an estimate of their importance in affecting breakdown where present information allows.

An important effect of the reentry induced hypersonic flow field is an apparent shift in altitude due to increased air density[52]. It is important to note that the air density is the proper independent variable in determining breakdown, rather than pressure, since the air is relatively warm.

Another effect of reentry is the change in gas composition. Due to the high levels of gas temperature and pressure resulting from the imparting of vehicle kinetic energy to its environment, the thermodynamic gas state for the reentry environment is significantly different from the room temperature state. This results in a shift in the population densities from N_2 and O_2 (principal constituents of room temperature air) to the dissociated forms NO and O (which occur in appreciable concentrations in a hypersonic cone boundary layer).[66] The resultant lowering of impact ionization potentials, which may be seen from the following brief table, will increase the ionization rate, enhancing breakdown.

Species	ev	$^{o}K \times 10^{-4}$
NO	9.25	10.7
O_2	12.2	14.2
N_2	15.6	18.1
N	14.5	16.8
O	13.6	15.8

An additional effect of the high temperature environment may be a substantial increase in attachment rate for the reentry environment.[66] Loss of electrons by attachment to molecular oxygen has been found to be most important relative to other constituents of air.[67] Epstein[66] notes that the cross section for this process may be significantly changed when oxygen is vibrationally excited at high temperature, resulting in a substantial increase in the attachment rate for the reentry environment.

The second main difference in the reentry environment is the presence of a significant level of ambient ionization. This increased ion population derives from three effects:

a. Intense heating in the bow shock wave and viscous boundary layer about the vehicle during hypersonic flight

b. Introduction of easily ionizable impurities in the flow field due to heat shield ablation

c. Ambient ionization of gases in the upper atmosphere.

These phenomena force reconsideration of two aspects of the breakdown analysis. The first aspect of the problem is simply the possibility of increasing the initial plasma frequency by virtue of the higher electron density such that it becomes an appreciable fraction of the applied signal frequency. This condition tends to shorten the time required to reach critical electron density and therefore breakdown. This factor must then be taken into account by adding a term to the electron continuity equation representing ionization rate in the absence of an electromagnetic field.[66] This term is determined by the flow field calculations which consider the thermal, ambient, and contaminant ionization rates as a function of gas state.

The second aspect of the existence of appreciable positive ion densities is to cause the diffusion process to become ambipolar rather than free as in the classical case.[66] Allis and Rose[68] have analyzed the transition from free to ambipolar diffusion. They indicate that the transition occurs when the Debye length for electrons becomes smaller than the diffusion length. Since ambipolar diffusion is slower than free diffusion by a factor of about forty[52], the rate of loss of free electrons will be reduced, resulting in a significant reduction in power required for breakdown.

Other terms which may be required for a description of reentry induced breakdown are the rates of recombination and detachment.[66] According to Lin and Tear[69] the dissociative recombination of electrons and nitric oxide ions (the most abundant ion present in high temperature air) proceeds at a rate of approximately $3 \times 10^{-3} T_e^{-3/2} cm^3/sec$. Epstein[66] shows that although according to the data of Muschlitz, detachment is negligible in the region from 3000° to 5000° K, further work is required before a definite conclusion can be made regarding the importance of detachment.

Another effect of reentry is the additional electron loss mechanism caused by the convection of air past the antenna. Kelly and Margenau[70] introduce this difference by noting that even for continuous wave breakdown the atmosphere is only subject to microwave heating for a time $\tau = L/V$ (L is the length of the antenna and V is the velocity of the antenna). Thus breakdown can occur only if the electron concentration becomes large enough in time τ since the antenna encounters a new enviroment every τ seconds. Fante,[71] in order to take account of this

effect, couples the velocity of the gas flowing past the antenna V with the electron continuity equation by rewriting the term dn/dt as $V \cdot \nabla n$. Kelly and Margenau[70] also redefine breakdown for a moving medium as that point in time when the signal frequency ω equals the plasma frequency ω_p. Epstein[66] points out that this definition is probably superior (though it is only approximately true) to the classical one where the power required for breakdown is defined as the incident power level which causes the net ionization rate to become positive. This classical definition fails to predict changes in the electron density if convection is present, and thus provides no information regarding the way in which the electron density approaches its final value.

Finally, the effect of nonuniform flow field distributions has been considered by Fante[71] in terms of its effect on the diffusion equation. This effect is taken into account by solving the diffusion equation for the given distribution of the diffusion coefficient.

It is probably best to calculate the effects of reentry on antenna breakdown by the phenomenological approach, rather than the kinetic theory approach. Classical breakdown in air, as discussed above, is successfully predicted on this basis. It should then be possible to formulate the approach in such a way as to obey a correspondence principle with respect to the classical limit. In other words, the results should approach the classical results when the reentry conditions become insignificant. This is probably most conveniently done by rewriting the continuity equation with additional terms representing each of the reentry effects, or with modified terms in certain cases.

3.4 NONLINEAR ATTENUATION AND DISTORTION

This section deals with the problem of interaction between a partially ionized plasma medium and incident high power radio-frequency electromagnetic radiation. The interaction induces a change in the equation of state of the plasma due to field energy coupling into the electron gas. As a result, the electron distribution function is altered and becomes dependent on the electric field intensity. Consequently, transport coefficients, such as thermal and electrical conductivities, which are deduced from the distribution function, become dependent on the local field intensities. While various forms of nonlinearities may be exhibited from the

interaction of electromagnetic radiation with a plasma, the particular class covered in this section is restricted to the case where the incident field deposits energy in the plasma and modifies the electron temperature, electron density, and effective collision frequency. The present interest is in the propagation of electromagnetic radiation in a plasma, and the conductivity coefficient is of paramount importance. More specifically, if f_e and f_i represent the electron and ion velocity distribution functions, then the components of the current j_k are related to the electric field components E_k by

$$j_k = -e\int f_e v_k \, d^3v + e\int f_i v_k \, d^3v = \sigma E_k. \tag{3.4-1}$$

In the above equation v_k is the k^{th} component of the velocity vector and σ is the scalar conductivity coefficient. In the presence of a magnetic field the scalar conductivity is replaced by a tensor conductivity coefficient. For most practical purposes the ion conduction current may be ignored and then Equation 3.4-1 is approximated by,

$$j_k = -e\int f v_k \, d^3 v = \sigma E_k. \tag{3.4-2}$$

In the preceding equation the subscript on the electron distribution function has been dropped for convenience. If the distribution function is a nonlinear function of the electric field intensity, the conductivity

$$\sigma = \frac{j_k}{E_k} = \frac{-e\int f v_k \, d^3 v}{E_k} \tag{3.4-3}$$

becomes a function of the electric field intensity.

In the following literature survey the electromagnetic-plasma nonlinear interactions will be grouped into three parts depending on the geometrical configuration of the plasma medium, namely, infinite, semi-infinite, and slab.

3.4.1 INFINITE PLASMA MEDIUM

The propagation of electromagnetic radiation in an unbounded nonlinear plasma medium excludes boundary effects and allows emphasis to be placed on the physics of the interaction process. An extensive investigation of this phase of the phenomena has been carried out by Ginzburg and Gurevich.[72] In fact, their paper provides an appropriate introduction and background to the entire field. They show that the nonlinear interaction of electromagnetic waves with partially ionized plasmas can be characterized in terms of several basic relaxation times. These are as follows:

τ = Electron density relaxation time

τ_{en} = Electron temperature relaxation time

T_{em} = $2\pi/\omega$ = Period of incident electromagnetic radiation

τ_{ee} = Relaxation time for the distribution function to become Maxwellian

τ_D = L^2/D = Characteristic diffusion time

L = Characteristic diffusion length

D = Diffusion coefficient

From the relative order of magnitude of the relaxation times it is possible to infer the specific nonlinear response of a plasma to intense electromagnetic radiation. Thus if

$$\tau \gg T_{em}, \tag{3.4-4}$$

$$\tau_{en} \gg T_{em}, \tag{3.4-5}$$

the electron density and temperature cannot follow the rapid variations of the electromagnetic field but assume a steady state value proportional to the mean square time average of the electric field. On the other hand if

$$\tau \ll T_{em} \tag{3.4-6}$$

$$\tau_{en} \ll T_{em} \tag{3.4-7}$$

then variations in electron density and temperature have ac components similar to those of the electric field intensity. This phenomenon exhibits the well known "Luxembourg" effect. A further subdivision of the response takes place depending on the relaxation time τ_{ee}, or the time required for the electrons to reach a Maxwellian distribution. Thus two possibilities exist depending on whether τ_{ee} is greater or less than the time required for the relaxation of electron temperature. A further subdivision depends on whether the electron density changes or is constant under the influence of the external field.

Ginzburg and Gurevich follow Allis[73] and obtain a solution to the Boltzmann equation by expanding the distribution function in a spherical harmonic series or

$$f = f_o + \frac{f_i' v_i}{w} + \text{---}, \tag{3.4-8}$$

where

f_o = Isotropic part of the distribution function

f_i = i^{th} component of the first spherical component of the distribution function

v_i = i^{th} component of electron velocity

w = Electron speed

It is found that when the thermal velocity is greater than the drift velocity, then it is sufficient to maintain only two terms in the series. It is advantageous to use the expansion in spherical harmonics rather than the perturbation method, since with the former technique it is possible to provide an accurate treatment of the energy dependence of the electron-neutral and electron-ion collisions for momentum transfer. By taking the steady-state case ($\partial f_o/\partial t = 0$) and the following collisions,

a. Elastic electron-neutral

b. Elastic electron-ion

c. Inelastic-neutral

d. Electron-electron

Ginzburg and Gurevich arrive at two expressions for the isotropic distribution function f_o for the electrons:

a. If $\tau_{ee} \ll \tau_{en}$ then f_o assumed a Maxwellian form.

b. If $\tau_{ee} \gg \tau_{en}$, then electron-electron collisions do not affect the form of f_o and

$$f_o = C \exp\left(-\int_o^w \frac{mw\,dw}{kT + e^2 E^2/3m\,G\left[\left(\omega^2 + \nu^2(w)\right)\right]}\right) \qquad (3.4\text{-}9)$$

Furthermore, when

$$e^2 E^2/3m\,G\left[\omega^2 + \nu^2(w)\right] \ll kT, \qquad (3.4\text{-}10)$$

Equation 3.4-9 reduces to a Maxwellian form. In the preceding equations G is the relative fractional loss of energy of an electron per inelastic collision (assumed small such as in

excitation of rotational or vibrational states) and T is the gas temperature. Equation 3.4-9 was originally derived by Margenau[74].

The ac conductivity is obtained from the first spherical harmonic component of the electron distribution function f_1', where

$$f_1' = \frac{-e E_i \partial f_o/\partial w}{m \left[\nu (w) - i \omega\right]} . \qquad (3.4\text{-}11)$$

Using Equation 3.4-2, the expression for the electron current density becomes,

$$j_i = -e \int f v_i d^3 v = -\left(\frac{4\pi}{3}\right) e \int_o^\infty f_1' w^3 dw = \sigma E_i \qquad (3.4\text{-}12)$$

From Equations 3.4-11 and 3.4-12,

$$\sigma = \left(\frac{4\pi}{3}\right)\left(\frac{e^2}{m}\right) \left[\int_o^\infty \frac{w^3 \nu (w) \partial f_o/\partial w}{\left(\omega^2 + \nu^2 (w)\right)} dw + i\omega \int_o^\infty \frac{w^3 \partial f_o/\partial w}{\left(\omega^2 + \nu^2 (w)\right)}\right] \qquad (3.4\text{-}13)$$

and

$$\nu (w) = \nu_{en} (w) + \nu_{ei} (w), \qquad (3.4\text{-}14)$$

where ν_{en} and ν_{ei} represent velocity dependent electron-neutral and electron-ion collisions.

Thus from Equation 3.4-13 if f_o is a function of the electric field intensity then σ, and therefore the propagation constant, is a function of E. The appropriate value for f_o is given by Equation 3.4-9 or the Maxwellian form at temperature T_e.

One of the earlier approaches to the nonlinear interaction problem was by Margenau.[74] He considered an infinite medium and arrived at the distribution function (isotropic) given by Equation 3.4-9 or

$$f_o = C \exp - \int_o^w \frac{mw\, dw}{kT + e^2 E^2/3m\, G\left[\omega^2 + \nu^2 (w)\right]} . \qquad (3.4\text{-}15)$$

Here τ_{ee} was taken greater than τ_{en} and interelectron collisions were not considered. The electron density was constant, and elastic-ion and inelastic electron-neutral collisions were ignored. Epstein[75] has also examined a similar problem.

Sodha and Palumbo[76] studied the propagation of an ellipitically polarized wave in a nonlinear homogenous, and unbounded magnetoplasma. The electron distribution function was not Maxwellian. Electron-ion and electron-electron collisions were not considered. Electron density was constant. The components of the conductivity tensor were found to be functions of the square of the local electric field amplitude.

Sodha and Palumbo[77] have also examined the problem where several electromagnetic waves propagate in an unbounded partially ionized plasma. The isotropic part of the electron distribution function was derived and found to be dependent on the frequency and square of the electric field amplitude for each wave. In the limit, for a single wave, the isotropic distribution function reduced to the case where only one wave is present. The conductivity depends on the frequency and square of the electric field amplitude for each wave present in the plasma. Thus the propagation characteristics of any single wave depend on the power density of the other waves propagating in the medium.

The problem of multi-frequency propagation has been considered by H. Mott[78] in conjunction with antenna breakdown in air. The breakdown depends not only on frequency but also on the envelope of the electric field. The envelope may be determined by phasor addition of the individual components. A minimum level is obtained for n equal amplitude signals by in-phase

addition. The resulting envelope peaks determine breakdown by acting as a continuous wave breakdown field, or if E_{eff} is the effective dc field,

$$E_{eff} = n E_o = E_{max}, \tag{3.4-16}$$

where E_o is the electric field intensity of each signal. The total minimum power for breakdown is given by,

$$P/P_{eff} = n \left(\frac{E_o}{E_{eff}} \right)^2 = 1/n \tag{3.4-17}$$

Additional work on multi-frequency signals has been carried out by Fante and Mullin[79]. Here an attempt is made to determine the effective electric field strength for a composite signal such as noise. For a stationary random signal E (t), the effective field is given by

$$E_{eff} = \left[\nu_c^2 \int_0^\infty \frac{S(f)\, df}{\omega^2 + \nu_c^2} \right], \tag{3.4-18}$$

where ν_c is the velocity independent collision frequency, and S (f) is the spectral density. The transmission of power by the noise signal is compared to that of a single frequency component. At high collision frequencies there is no difference between the signals. However, when $\nu_c \leq \omega_o$ the single frequency can transmit more power than the noise signal. Here $\omega_o = (\omega_1 + \omega_2)/2$, where ω_1 and ω_2 represent the upper and lower cutoff frequencies.

3.4.2 SEMI-INFINITE PLASMA

The interaction of electromagnetic radiation with a semi-infinite plasma introduces boundary phenomena and facilitates the analytical investigation of the behavior of spatial inhomogeneities in the plasma. This problem was considered by King[80], Yen[81], and Papa[82,83]. The result of the perturbation (electric field) modifies the boundary between the nonionized and ionized

medium in such a way that it appears to move towards the radio frequency source. The electron temperature and electron density become functions of both time and space. King and Yen make use of the time-independent WKB approximation. They assume that the isotropic part of the electron velocity distribution function is Maxwellian, but do not account for the velocity dependence of the electron-neutral cross sections. No heat conduction in the electron gas is assumed. Papa's analysis is based on the three moments of the Boltzmann equation for the electron gas. The moment equations are truncated by setting the heat flow vector proportional to the temperature gradient. The relaxation time is short enough for f_o to remain Maxwellian. Ionization by electron impact on neutrals, electron-electron attachment, and electron-ion recombination are included in the analysis. The conductivity is given by Equation 3.4-13. The continuity and energy balance equations are solved numerically for the electron density N_e and temperature T_e. It is also shown by Papa that the time scale τ_{en} is much shorter than τ.

Dysart[84] applied the theoretical approach given by Papa[82,83] and obtained numerical solutions to the time dependent problem. His results almost completely duplicate Papa's original presentation. Extensive graphical data is presented.

Epstein[85] treated the semi-infinite problem for a chemically reacting and inhomogeneous plasma medium. He did not take into account electron-ion collisions, and the velocity dependence of electron-neutral collisions, and the form of the distribution function. He assumed that the ratio of electromagnetic energy transferred to the plasma to the internal energy (shock induced) was small and thereby linearized the fluid dynamical and chemical equations. Under these somewhat restricted conditions he showed that a small electromagnetic field produced substantial changes in the reflection coefficients.

Papa[86] has also considered the case where a dc magnetic field is imposed parallel to the electron density gradient. Time dependence was taken into account. He showed that gradients in electron density cause the incident field to experience frequency shift. The frequency shift of the left-hand circularly polarized wave differs from the frequency shift of the right-hand wave. Dysart[84] has also supplemented this work by performing numerical computations.

3.4.3 PLASMA SLAB

The nonlinear interaction between electromagnetic radiation and an inhomogeneous plasma slab represents a problem which in many ways closely simulates practical conditions. Papa and Case[87] have examined the steady-state nonlinear response of an inhomogeneous plasma slab when illuminated by intense plane wave radiation. The constituents were selected to correspond to those of air behind a strong shock. The constituents included are the neutrals N_2, NO, N, and O. It is shown that for a large range of shock parameters $\tau_{ee} \ll \tau_{en}$, $\tau_{ee} \ll \tau_D$, and f_o is Maxwellian. Thus the rate coefficients can be defined in terms of an electron temperature T_e. The energy balance equation is solved numerically and the results plotted graphically for T_e versus E^2/ω^2. It is shown that it is possible to have multivalued solutions of T_e for certain ranges of E^2/ω^2. In this range the electron gas can exist in three temperature states. The reflection and transmission coefficients were computed by Papa and Case employing the Runge-Kutta technique to integrate Maxwell's equations. The reflection coefficient is presented as a function of E_{inc}^2/ω^2 for several values of $\omega_{p(max)}/\omega$. Here E_{inc} is the incident field and $\omega_{p(max)}$ is the maximum plasma frequency of the initial electron density profile. It is found that the reflection coefficient is relatively constant until a critical value is reached corresponding to the electron avalanche. At this point the reflection coefficient increases sharply while the transmission coefficient drops to low values.

Dysart[84] has obtained numerical solutions for electromagnetic transmission through a plasma slab under steady state conditions. The plasma is taken as inhomogeneous and isotropic with parameters corresponding to the flow around a blunt vehicle travelling at 18,000 ft/sec at an altitude of 200,000 feet. The constituents are N_2 NO, and O at 5000°K. The radio frequency is taken much greater than collision frequencies so that the conductivity given by Equation 3.4-13 reduces to,

$$\sigma = \frac{N_e e^2 \nu_{eff}}{m\omega^2} + i\frac{N_e e^2}{m\omega}, \qquad (3.4\text{-}19)$$

and

$$\nu_{eff} = \frac{\sqrt{2}}{3\sqrt{\pi}} \left(\frac{m}{k T_e} \right)^{5/2} \int_0^\infty \nu(w) w^4 \exp\left(- \frac{mw^2}{2k T_e} \right) dw, \qquad (3.4\text{-}20)$$

with

$$\nu_{eff} = \sum_j \nu_i (T_e) + \nu_{ion} (T_e), \qquad (3.4\text{-}21)$$

where $\nu_j (T_e)$ is the effective collision frequency for the component of the neutral constitutent. Numerical data is presented graphically and includes reflection and transmission coefficients. The effort by Dysart[84] is strictly computational and the theory is identical to that presented by Papa and Case[87].

The case of propagation through an inhomogeneous, nonlinear magnetoactive plasma slab for time invariant electron density was examined by Papa[88]. The components of the conductivity tensor are functions of the power density of three modes, namely, right-hand, left-hand, and longitudinal. For normal incidence an elliptically polarized incident field launches only a right-hand and a left-hand mode into the plasma for a dc magnetic field parallel to the electron density gradient. These two modes are uncoupled at low power. At higher input power, the modes do not propagate independently of one another. If desired, it is possible to compute the net reflection and transmission coefficients for the left- and right-hand modes.

3.5 ALLEVIATION TECHNIQUES

Some methods of alleviating reentry communications blackout are briefly surveyed, including aerodynamic shaping, reducing the free electron density, and altering the propagation properties of the plasma.

The general principle in aerodynamic shaping is either to locate the antenna outside of the plasma sheath or to modify the flow field so that the plasma density is reduced in the vicinity

of the antenna. Three techniques are compared in Reference 89. The communications fin is a narrow angle wedge fin projecting beyond the bow shock of the vehicle. Since the fin is narrow, the plasma generated by it is weak compared to the plasma generated by a blunt vehicle. Thus if the antenna system were located on the fin, the effects of plasma attenuation could be alleviated. The problems involved include structural stability of the fin, and aerodynamic stability of the vehicle with such a fin.

The aerospike antenna is a narrow antenna projecting into the plasma sheath. A coolant is injected into the flow stream upstream of the antenna.

Flow diverters are small projections from the vehicle into the flow stream which would modify the flow stream so that the sheath thickness over the area of the antenna is reduced. Flow diverters would be lighter than the two previously mentioned techniques, and would require less modification to existing vehicle designs.

Reference 89 also considers plasma alleviation by coolant injection. Among various materials considered, water was chosen as most effective. The jet of water would be shot normal to the surface of the vehicle. A shock would form because of the interaction of the jet and the flow field, and the jet would break up into droplets. The water would then cool the plasma by evaporation.

Ohio State's Electro-Science Laboratory[90] is designing a system which would project a jet of cool gas ahead of the vehicle. Not only would this system cool the plasma formed, but it would also protect the vehicle since the shock would form on the tip of this jet, rather than on the nose of the vehicle. The gas spike is to be tested on a trailblazer vehicle.

The injection of an electronegative gas such as SF_6 could have three desirable effects as follows: (1) it would act as a coolant because of the heat of dissociation of SF_6 into its component atoms. (2) It could reduce the equilibrium concentration of free electrons due to attachment. (Good[91] points out that the predominant mechanism is actually a three-body reaction where the third body carries off the excess association energy.) (3) It serves as a

catalyst for air recombination. Thus it can be used in conjunction with another coolant to hasten equilibrium.

Reference 89 also considered injecting dust into the plasma, so that the dust particles could serve as nuclei for electrons to collect on. One dust particle could clean out a volume with a radius of one Debye length. Since the smallest particle which could be easily handled was thought to be on the order of 1 micron, it was concluded that other methods would weigh less.

Attenuation for right-hand circularly polarized waves propagating normal to a plasma layer will be reduced in the presence of a magnetic field in the direction of propagation. This is because the Lorentz force checks the ability of the electron generated field to cancel the imposed field. Rothman and Morita[92] consider the problem analytically for rectangular coordinates. The conditions for enhancement are that the electron cyclotron frequency be greater than the imposed angular frequency, and that the square of the collision frequency be much less than the square of the difference between the cyclotron frequency and the imposed angular frequency. Rothman and Morita carried out experimental laboratory work using an RF discharge which demonstrated qualitative enhancement and polarization in the presence of a magnetic field.

Samaddar[93,94] considers magnetic window effects in special cases of nonrectangular geometries. In particular, he considers cylindrical and conical geometries which approximate vehicle shapes. His method utilized calculating the dielectric tensor as a function of the applied magnetic field, and the plasma and collision frequencies. To gain effective control over attenuation, mutual orientation of the antenna and imposed magnetic field must be chosen so that the field components are independent of components of the dielectric tensor parallel to the imposed magnetic field. This approach has been analyzed[89] in terms of weight requirements and found to be feasible only if a greater system loss figure than with the other alleviants (20 db rather than 10 db) could be tolerated. The use of superconducting magnets has some promise for short flights, but cooling equipment becomes a limiting factor.

A critical analysis of these and other techniques should be made before any firm conclusions can be drawn. Fluid mechanic effects of shaping and additives will be considered more systematically in future reports. Alleviation of antenna breakdown will be given more emphasis also.

SECTION 4
CONCLUSION

It has been determined that the construction of an accurate nonequilibrium flow field is possible through the judicious use of the nonequilibrium streamtube solution in conjunction with a perfect gas or equilibrium flow field solution. The method is approximate only to the extent that the bow shock and streamwise pressure distributions are approximate.

The problem of analyzing antenna near-field distributions cannot be set up in a perfectly general way which will give good results in a variety of cases. However, the general approaches used in the theory of the linear antenna provide a good basis for approximate approaches to more general problems.

A good deal of applicable literature exists on the linear effects of plasma on antenna impedance and pattern distortion. Some of these theories could prove useful in making parametric calculations.

The prediction of antenna breakdown by the kinetic theory approach is not feasible except for certain ideal cases. Phenomenological theories have succeeded in predicting the results of experiment for static breakdown in air. Whether or not the phenomenological theory can be extended to cover the effects of reentry remains to be seen.

Nonlinear plasma effects and some techniques for alleviation of linear plasma effects have been surveyed. Assessment of the importance of these two technical areas with respect to the present application must await further evaluation.

SECTION 5
REFERENCES

1. Gravalos, F.G., Edelfelt, I.H., and Emmons, H.W. "The Supersonic Flow About a Blunt Body of Revolution for Gases at Chemical Equilibrium." 9th Annual Congress of International Astronautical Federation, Amsterdam, August, 1958.

2. Jones, D.W. and Friedhofer, J. "A Description of the Use of MSD IBM Program DPC 7M.1, Entitled 'Characteristic Solution of Supersonic Flow'." GE-MSD Report TIS R59SD399, October 1958.

3. Edsall, R.H. "A Modified Method of Characteristics for Calculating Inviscid Flow Fields." GE-MSD Fluid Mechanics Fundamentals Memorendum 101, March 1963.

4. Hilsenrath, J. and Beckett, C.W. "Tables of Thermodynamic Properties of Argon-Free Air to 15,000°K." National Bureau of Standards, Washington, D.C., September 1956.

5. McMenamin, D.L. and O'Brien, M. "The Finite Difference Solution of Multicomponent Non-Equilibrium Steady Influscid Streamtube Flows Using A Novel Stepping Technique. Part I Analysis and Applications." General Electric Company, TIS 67SD241, April 1967.

6. Lin, S.C., Neal, R.A. and Fyfe, W.I. "Rate of Ionization Behind Shock Waves in Air. I. Experimental Results." AVCO/Everett Research Report 105, September 1960.

7. Kaegi, E.M. and Chin, R. "Stagnation Region Shock Layer Ionization Measurements in Hypersonic Air Flows." AIAA Preprint 66-167, 1966.

8. Gravalos, F.G. and Studerus, C.J. "Inviscid Non-Equilibrium Flow Along a Surface of a 45^{o} Cone." General Electric Company, PIR 8152-2127, December 1966.

9. Silver, S. Microwave Antenna Theory and Design. McGraw-Hill, New York, 1949 (Ch. 3).

10. Walter, C.H. Travelling-Wave Antennas. McGraw-Hill Book Co., 1964.

11. Collin, R.E. Field Theory of Guided Waves, McGraw-Hill Book Co., 1960, p. 401.

12. Ramo, S. and Whinnery, J.R. Fields and Waves in Modern Radio, John Wiley & Sons, p. 410, 1959.

13. Watkins, D.A. Topics in Electromagnetic Theory. John Wiley & Sons, 1958.

14. Neurather, A.R., et al. "A Study of the Sheath Helix with a Conducting Core and its Application to the Helical Antenna." Trans. IEEE, Vol. AP-15, p. 203, March 1967.

15. King, R.W.P. Theory of Linear Antennas. Harvard University Press, 1956.

16. Hallen, E. "Theoretical Investigations into the Transmitting and Receiving Qualities of Antennas." Nova Acta Regiae Soc. Upsaliensis, Sec. IV, Vol. II, p. 1; 1938.

17. Kraus, J.R. Antennas. McGraw-Hill Book Co.

18. King, R.W.P., and Middleton, D. "The Cylindrical Antenna: Current and Impedance." Quart. Appl. Math., Vol. 3, p. 302, 1946.

19. King, R.W.P., and Wu, T.T. "Currents, Charges, and Near Fields of Cylindrical Antennas." Radio Science, Vol. 69D, p. 429, March, 1965.

20. King, R.W.P., and Harrison, C.W. Jr., "The Distribution of Current Along a Symmetrical Center-Driven Antenna." Proc. IRE, Vol. 31, p. 548, 1943.

21. King, R.W.P., and Wu, T.T. "The Imperfectly Conducting Cylindrical Antenna." Trans. IEEE Ant. & Prop., Vol. AP-14, p. 524, September 1966.

22. Balmain, K.G. "Impedance of a Short Dipole in a Compressible Plasma."

23. Cook, K.R., and Edgar, B.C. "Current Distribution and Impedance of a Cylindrical Antenna in an Isotropic Compressible Plasma." Radio Science, Vol. I, p. 13, January 1966.

24. Iizuka, K., King, R.W.P., and Harrison, C.W. Jr., "Self and Mutual Admittances of Two Identical Circular Loop Antennas in a Conducting Medium and in Air." Trans. IEEE, Vol. AP-14, p. 440, July 1966.

25. Wait, J.R., "The Electromagnetic Fields of a Dipole in the Presence of a Thin Plasma Sheet." Appl. Sci. Res., Sec. B, Vol. 8, p. 397, 1960.

26. Tamir, T., and Oliner, A.A. "Guided Complex Waves," Proc. IEEE, Vol. 110, p. 310, February 1963. Also, "The Spectrum of Electromagnetic Waves Guided by a Plasma Layer," Proc. IEEE, Vol. XXX, p. 317, 1963.

27. Wenger, N.C. "Radiation from a Slot Antenna in a Ground Plane Covered by a Warm Plasma Layer," NASA TN-D-3504, July 1966.

28. Bernard, G., and Ishimaru, A. "Pole Contributions to Electromagnetic Fields in the Light of a Modified Saddle-Point Technique." U. of Washington, Dept. of EE, Report 82; October 1963, AD 427361.

29. Harrington, R.F. Time-Harmonic Electromagnetic Fields, McGraw-Hill, 1961 (Ch. 7).

30. Banos, A. Jr., Dipole Radiation in the Presence of a Conducting Half-Space, Pergamon Press, 1966.

31. Watson, G.N. "The Diffraction of Electric Waves by the Earth." Proc. Roy. Soc., Vol. A95, p. 83, 1918.

32. Sommerfeld, A. Partial Differential Equation. Academic Press, Inc., p. 214, 1949.

33. Wait, J.R. "Electromagnetic Surface Wave." Advances in Radio Research, Vol. 1, p. 157, Academic Press, Inc., 1964.

34. Bremmer, H. Terrestial Radio Wave. Elsevier Co., 1949, p. 12.

35. Wait, J.R. and Spies, K.A. "Radiation from a Slotted Sphere Antenna Covered by a Plasma Layer." Radio Science, Vol. 69D, 1965.

36. Yeh, C. "On the Dielectric Coated Prolate Spheroidal Antenna." J. Math and Phys., Vol. 42, p. 68, 1963.

37. Smith, T.M. and Golden, K.E. "Radiation Patterns from a Slotted Cylinder Surrounded by a Plasma Sheath." IEEE Trans. Ant. & Prop., Vol. AP-13, p. 775, 1965.

38. Swift, C.T. "Radiation from Slotted Cylinder Antennas in a Re-entry Plasma Environment." NASA TN D-2187, 1964.

39. Rusch, W.V.T. "Radiation from a Plasma Clad Axially-Slotted Cylinder." USCEC Report 82-201 (AECRL 714), Univ. of S. Cal., May 1962.

40. Knop, C.M. "Radiation Fields from a Circumferential Slot on a Metal Cylinder Coated with a Lossy Dielectric." IRE Trans. Ant. & Prop., Vol. AP-9, p. 535, 1961.

41. Harris, J.H. "Radiation through Cylindrical Plasma Sheaths." Electromagnetic Aspects of Hypersonic Flight. W. Rotman, Spartan Books, p. 89, 1964.

42. Sengupta, D.L. "The Radiation Field Produced by an Infinite Slot in an Infinite Cylinder Surrounded by a Homogeneous Plasma Sheath." Univ. of Michigan, Report 4563-35-T, May 1963.

43. Harley, T.P. and Tyras, G. "Transmission of Electromagnetic Waves Through an Ionized Layer in the Presence of a Strong Magnetic Field." Proc. IRE, Vol. 49, p. 1822, 1961.

44. Richmond, J.H. "Transmission through Inhomogeneous Plane Layers." IEEE Trans. Ant. & Prop., Vol. AP-10, p. 300, May 1962.

45. Swift, C.T. and Evans, J.S. "Generalized Treatment of Plane Electromagnetic Waves Passing through an Inhomogeneous Plasma Slab at Arbitrary Angles of Incidence," NASA TR R-172, 1963.

46. Yeh, C. "An Application of Sommerfeld's Complex Order Wavefunctions to an Antenna Problem." J. Math. Phys., Vol. 5, p. 344, 1964.

47. Banos, A. et al. "The Radiation Field of an Electric Dipole Antenna in a Conical Sheath." J. Math. & Phys., Vol. 70, p. 189, 1965.

48. Jordan, A.K. et al. "Antenna Pattern Distortion by a Conical Plasma Sheath with Electron Collisions." General Electric Report, TIS 67SD218, 3 April 1967.

49. Pridmore-Brown, D.C. "Electric Dipole Radiation through a Finite Conical Plasma Sheath." IEEE Trans. Ant. & Prop., Vol. AP-14, p. 428, July 1966.

50. Menzel, D.H. "Some Problems of Ionospheric Non-linearities." Radio Science, Vol. 69D, p. 1, 1965.

51. Chen, K.M. "Interaction of a Radiating Source with a Plasma." Univ. of Michigan, Report 4563-39-T, AD 413324.

52. MacDonald, A.D. Microwave Breakdown in Gases. John Wiley & Sons, New York, 1966.

53. Chapman, S. and Cowling, T.G. The Mathematical Theory of Non-Uniform Gases. Cambridge University Press, Cambridge, 1960.

54. Kihara, T. "The Mathematical Theory of Electrical discharges in Gases." Rev. Mod. Phys., Vol. 24, No. 1, January 1952.

55. MacDonald, A.D. and Brown, S.C. Phys. Rev., Vol. 75, p. 411, 1949.

56. MacDonald, A.D. and Brown, S.C. Phys. Rev., Vol. 76, p. 1634, 1949.

57. Reder, F.H. and Brown, S.C. Phys. Rev., Vol. 95, p. 885, 1954.

58. Herlin, M.A. and Brown, S.C. Phys. Rev., Vol. 74, p. 291, 1948.

59. Herlin, M.A. and Brown, S.C. Phys. Rev., Vol. 74, p. 1650, 1948.

60. MacDonald, A.D. and Brown, S.C. Can. J. Res., Vol. A28, p. 168, 1950.

61. Brown, S.C. Basic Data of Plasma Physics, MIT Press, Cambridge, Mass., 1966.

62. Rose, D.J. and Brown, S.C. J. Appl. Phys., Vol. 28, p. 561, 1957.

63. Gould, L.J. and Roberts, L.W. J. Appl. Phys., Vol. 27, p. 1162, 1956.

64. Harrison, M.A. and Geballe, R. Phys. Rev. Vol. 91, p. 1, 1953.

65. MacDonald, A.D., Gaskell, D.U., and Gitterman, H.N. Phys. Rev., Vol. 130, p. 1841, 1963.

66. Epstein, M. "Antenna Breakdown in a Hypersonic Re-entry Environment." SSD-TR-65-140, TDR-669(6240-20)-1, AD473936, September 1965.

67. Biondi, M.A. Advances in Electronics and Electron Physics, Vol 18, p. 67, 1963.

68. Allis, W.P., Rose, D.A. "The Transition from Free to Ambipolar Diffusion," Phys. Rev., Vol. 93, No. 1, 1 January 1954.

69. Lin, S.C. and Teare, J.D. "Rate of Ionization Behind Shock Waves in Air. II." AFCRL-62-751, Avco Research Report 115.

70. Kelly, D., Margenau, H. "High Frequency Breakdown of Air." J. Appl. Phys., Vol. 31, No. 9, September 1960.

71. Fante, R.L. "Mathematical Analysis of Microwave Breakdown in Flowing Gases." IEEE Trans. on Ant. and Prop. pp. 781-788, September 1965.

72. Ginzburg, V.L. and Gurevich, A.V. USP. Fiz. Nauk. Vol. 70, p. 201, 1960.

73. Allis, W.P. Handbuch der Physik, Vol. 21, Springer-Verlag, 1956.

74. Margenau, H. Phys. Rev. Vol. 69, p. 508, 1946.

75. Epstein, M. Phys Fluids, Vol. 3, p. 1016, 1960.

76. Sodha, M.S. and Palumbo, C.J. Can. J. Phys. Vol. 41, p. 1702, 1963.

77. Sodha, M.S. and Palumbo, C.J. Can. J. Phys. Vol. 41, p. 2155, 1963.

78. Mott, H. Proc. IEEE, Vol. 52, p. 1752, 1964.

79. Fante, R.L. and Mullin, C.R. Proc. IEEE, Vol. XXX, p. 484, 1965.

80. King, J.I.F. RADC-TDR-62-48A, 1962.

81. Yen, K.T. Phys. Fluids, Vol. 7, p. 1612, 1964.

82. Papa, R.J. Can J. Phys., Vol. 43, p. 38, 1965.

83. Papa, R.J. Phys. Fluids, Vol. 8, p. 1408, 1965.

84. Dysart, L.A. A.S. Thomas Inc. Report, May 1966.

85. Epstein, M. Phys. Fluids, Vol. 7, p. 121, 1964.

86. Papa, R.J. AF CRL-65-51, 1965.

87. Papa, R.J. and Case. Can. J. Phys. Vol. 43, p. 2021, 1965.

88. Papa, R.J. Proc. of the Third Symposium on the Plasma Sheath, Plasma Electromagnetics of Hypersonic Flight.

89. "Lifting Re-entry Communications, Vol. I." Aerospace Report TR-669(6220-10)-3, Vol. 1, Air Force Report SSD-TR-66-73, Vol. 1, Aerospace Corporation, Re-entry and Plasma-Electromagnetics Department. 1 May 1966.

90. "Aerodynamic Gas Spike for Re-entry Vehicle Communications Studies," Interim Technical Report 2010-7, 7 March 1967; and Technical Report 2010-6, 1 November 1966, Electro-Science Laboratory, The Ohio State University.

91. Good, Earl R., (Mithras, Inc.). "Electron Attachment to Atomic Fluorine in Thermally Ionized Air." NASA Contractor Report NASA CR-516, July 1966.

92. Rothman, H., and Morita, T. (Stanford Research Institute). "Transmission Through an Ionized Medium in the Presence of a Strong Magnetic Field." Air Force Cambridge Research Laboratories Technical Report 74, May 1961.

93. Samaddar, S.N. "An Approach to Improve Re-entry Communications by Suitable Orientations of Antenna and Static Magnetic Field." Radio Science Journal of Research, Vol. 69D, No. 6, pp. 851-863, June 1965.

94. Samaddar, S.N. "Principle of Blackout Communications" AIAA Journal, Vol. 3, No. 2, pp. 349-351.

Unclassified
Security Classification

DOCUMENT CONTROL DATA - R&D

(Security classification of title, body of abstract and indexing annotation must be entered when the overall report is classified)

1. ORIGINATING ACTIVITY (Corporate author)
General Electric Company
Reentry Systems Dept., Missile & Space Div.
Box 8555, Philadelphia, Pennsylvania 19101

2a. REPORT SECURITY CLASSIFICATION
Unclassified

2b. GROUP

3. REPORT TITLE

STUDY TO OBTAIN DESIGN DATA FOR REENTRY ECM ANTENNA SYSTEMS

4. DESCRIPTIVE NOTES (Type of report and inclusive dates)
Scientific. Interim.

5. AUTHOR(S) (First name, middle initial, last name)
Paul E. Bisbing Walter Sawchuk
Arthur K. Jordan Paul M. Scherer
Daniel L. McMenamin

6. REPORT DATE
June 1967

7a. TOTAL NO. OF PAGES
110

7b. NO. OF REFS
34

8a. CONTRACT OR GRANT NO.
F 19(628)-67-C-0210

ARPA Order No. 693 Amend. No. 1

b. PROJECT
8671

c. DOD ELEMENT 625G301R

d. DOD SUBELEMENT None

9a. ORIGINATOR'S REPORT NUMBER(S)
GE Report 67SD5232

First Quarterly Technical Report Vol. 1 of 2

9b. OTHER REPORT NO(S) (Any other numbers that may be assigned this report)
AFCRL-67-0473

10. DISTRIBUTION STATEMENT
This document is subject to special export controls and each transmittal to foreign governments or foreign nationals may be made only with the prior approval of, AFCRL (CRDM), L. G. Hanscom Field, Bedford, Massachusetts 01730

11. SUPPLEMENTARY NOTES
This research was sponsored by the Advanced Research Projects Agency

12. SPONSORING MILITARY ACTIVITY
Air Force Cambridge Research Laboratories (CRD)
L. G. Hanscom Field
Bedford, Massachusetts 01730

13. ABSTRACT

This report is the first quarterly technical report under this study of reentry effects associated with the transmission of electronic countermeasure (ECM) signals. Illustrative results for the aerothermochemical properties are presented for typical slender-body reentry conditions. These results were obtained from an approximate nonequilibrium inviscid shock layer flow field solution, which utilizes a combination of reacting streamtube and equilibrium flow field solutions. A discussion of the calculation method is included.

Literature surveys in the area of theory of antennas and propagation are summarized. (Types of ECM antennas in common use are discussed in Volume II.) Methods of calculating near-field distributions of antennas are discussed in a general way. Theoretical analyses of linear plasma effects are surveyed. Antenna breakdown is considered in terms of both the static air environment and the reentry environment. The theories of nonlinear propagation effects are summarized and finally a review of some alleviation techniques is given.

In general, it appears that nearly all of the important reentry effects on antennas and propoagation can be reasonably well characterized using existing theory. However, parametric evaluation using these theories will have to be completed before this conclusion can be affirmed.

DD FORM 1 NOV 65 1473

Unclassified

14. KEY WORDS	LINK A		LINK B		LINK C	
	ROLE	WT	ROLE	WT	ROLE	WT
Bibliography/Analytical Techniques Reentry Plasma Flow Field Antenna Near Field Plasma Attenuation Antenna Breakdown						